Nanoscale

REVIEW

View Article Online
View Journal | View Issue

Cite this: *Nanoscale*, 2025, **17**, 27734

Magnetic hyperthermia in focus: emerging non-cancer applications of magnetic nanoparticles

Helena Gavilán, *†[a] Alvaro Gallo-Cordova, *†[b] Maura Rábade-Chediak, [c] Amira Páez-Rodríguez, [c] María del Puerto Morales [b] and Lucía Gutiérrez *[c,d]

Magnetic hyperthermia (MH), which leverages the ability of magnetic nanoparticles (MNPs), located in the tumor, to generate heat upon exposure to an alternating magnetic field (AMF), has long been synonymous with cancer therapy. However, recent advancements highlight emerging applications of MH beyond oncology, including neuromodulation, tissue engineering, biosensing, catalysis, and environmental remediation. All these applications intelligently harness the same principle to achieve a wide range of new functionalities in MNPs besides local heating, including drug release, eradication of pathogens, manipulation of cell membranes, mechanical responses for novel non-invasive therapies, boosting chemical reactions, intensifying processes and degrading or desorbing pollutants like CO_2, just to name a few. This review provides a comprehensive overview of the latest breakthroughs in non-cancer applications of MH. While some fields, ranging from infection control and organ cryopreservation to nanorobotics in biomedicine, require non-toxic biocompatible and biodegradable MNPs (iron oxides) and AMFs restricted to radiofrequencies in the range of 100–300 kHz and an appropriate field intensity (few tens of kA m^{-1}) to avoid tissue damage, some other areas, like sustainable catalysis, sensing, *etc.*, open up the possibility of using diverse chemical elements besides iron (*e.g.*, cobalt, nickel, carbon) mainly in the form of alloys, and AMFs of higher frequencies (well above 300 kHz) and amplitudes (well above 10–20 kA m^{-1}). Indeed, engineering of MNPs with suitable catalytically active elements (gold, nickel, ruthenium, palladium, *etc.*), support materials (silica, aluminium/magnesium oxide, *etc.*) or surface coating with appropriate (bio) molecules (enzymes, RNA/DNA fragments, *etc.*) is crucial for each application, as well as considering the effect of local temperature (for instance, achieving the Curie temperature, T_c, of the nanomaterial, provoking the de-swelling of polymers, activating/deactivating enzymes or boosting the efficiency of a catalytic process). Furthermore, this work discusses the current limitations and future directions required to expand the reach of MH. Finally, this review serves as a critical resource for researchers seeking to harness MH beyond cancer treatment and integrate it into novel scientific and technological frontiers.

Received 6th August 2025,
Accepted 25th October 2025

DOI: 10.1039/d5nr03329b

rsc.li/nanoscale

1. Introduction

Magnetic hyperthermia (MH) was initially conceived for therapeutic purposes using magnetic nanoparticles (MNPs) (in particular superparamagnetic iron oxide nanoparticles, SPIONs like magnetite and maghemite) to generate localized heat when exposed to alternating magnetic fields (AMFs).[1,2]

All the research performed on MH in the past decades has driven us towards a better understanding of heat generation by SPIONs and Néel and Brownian relaxation in response to AMFs.[3] Novel approaches have been proposed for the reliable determination of the heating capacity of the particles when exposed to an alternating magnetic field, usually described as the specific loss power (SLP), the intrinsic loss power (ILP) or the specific absorption rate (SAR), which represents the amount of energy absorbed per unit of mass in the presence of an AMF and can be measured in units of watts per gram of metal (W g^{-1}).[4–6] Importantly, some of these works are interlaboratory studies, which reveal ongoing challenges in achieving consistent MH measurements and stress the need for standardization.[5] Other interesting topics that have been developed during the study of local heat generation are nanothermometry[7–10] (or the use of non-invasive precise thermometers working at the nanoscale) and an understand-

[a]*Departamento de Química Física, Universidad Complutense de Madrid, Madrid 28040, Spain. E-mail: hgavilan@ucm.es*
[b]*Instituto de Ciencia de Materiales de Madrid (ICMM-CSIC), Madrid 28049, Spain. E-mail: alvaro.gallo@csic.es*
[c]*Instituto de Nanociencia y Materiales de Aragón (INMA), CSIC-Universidad de Zaragoza, Zaragoza 50009, Spain. E-mail: lu@unizar.es*
[d]*CIBER-BBN, Zaragoza 50009, Spain*
†These authors contributed equally.

ing of how viscosity or complex biological media may change the dissipation of heat locally.[11,12]

Advancements in MNP designs have led to SPIONs, as well as other MNPs with diverse chemical compositions and morphologies, capable of maximizing localized heat. In parallel, diverse AMF applications have been developed, opening the possibility of employing MH for other purposes besides cancer therapy. Indeed, the restrictions of *in vivo* applications, which require non-toxic, biocompatible and biodegradable MNPs and AMFs limited to radiofrequencies in the range of 100–300 kHz and an appropriate field intensity (few tens of kA m^{-1}) (to avoid tissue damage), disappear for other *ex vivo* applications. Moving outside *in vivo* applications enables the use of cobalt, nickel and carbon alloys, among others,[13] AMFs well above 300 kHz and amplitudes well above 10–20 kA m^{-1}. Complex compositions may include gold,[14] nickel,[15] ruthenium,[16] and palladium,[17] *etc*., support materials (such as silica,[17] aluminum/magnesium oxide,[18] *etc*.) or (bio)molecules (enzymes,[19] RNA/DNA fragments,[20] *etc*.).

As a result of all these advancements, MH has become more expansive technology and the principles of localized heating through exposure to AMFs are being used for the development of many biomedical applications beyond oncology, offering innovative solutions in various fields. This review explores such promising applications, including, among others, MH treatment for bacterial infections,[21] on-demand drug release,[22] or treatment for cardiovascular diseases.[23]

Moreover, MH has also been used in other applications completely unrelated to biomedicine. Recent works have proposed the use of magnetic induction heating as part of nanocatalysis processes.[24] In addition, MH was recently employed to modify the viscosity of crude oils in the frame of petroleum associated technologies[25] or to induce the degradation of organic pollutants.[26]

In summary, the possibilities for MH in a wide range of completely different applications are endless and we have only scratched the surface of its incredible potential. Therefore, the main aim of this review is to provide an overview of the different possible uses of MH that have arisen in the past years beyond the more widely studied cancer treatment.

2. Basic concepts: a guided overview

MH is governed by a complex interplay of magnetic relaxation dynamics, nanoparticle properties, and environmental conditions. To provide a clear framework for understanding its fundamental principles, this section is structured around a series of conceptual questions that highlight the key physical and operational parameters influencing heat generation at the nanoscale. Through this question-driven approach, essential aspects such as the distinction between magnetic and conventional heating, relaxation mechanisms in different media, safety limits for biomedical applications, and metrics for evaluating heating performance are discussed.

This format facilitates a focused introduction to the core concepts relevant to both a theoretical understanding and the practical implementation of MH.

2.1 What makes MH fundamentally different from conventional heating?

MH relies on the ability of MNPs to dissipate energy as heat when subjected to an AMF. Unlike traditional bulk heating methods, which heat the entire medium uniformly, MH offers localized heating, particularly relevant in microenvironments where temperature gradients can drastically affect reactivity and biological outcomes.

This distinction between bulk heating and localized MH is central to understanding the advantages and limitations of each approach in both biomedical and non-biomedical contexts. Bulk heating methods (*e.g.* oil baths, resistive heaters, or convective ovens) transfer thermal energy to the system primarily through conduction and convection. This mode of heating generates large thermal gradients at the macroscopic scale, as energy is transferred from an external source to the system *via* conduction and convection.[27] As a consequence, regions closer to the heat source can become overheated while more distant or internal areas remain significantly cooler, often resulting in uneven temperature profiles. This can be inefficient in systems involving temperature sensitive components, where precise thermal control is required.

In contrast, MH exploits the ability of MNPs to act as nanoheaters that dissipate energy locally upon exposure to an AMF by generating hot-spots. Heating is restricted to the immediate nanoscopic environment of the particles.[28] This spatial confinement allows for highly localized thermal gradients, enabling selective activation of thermally driven processes, such as catalytic reactions,[29,30] without the need to elevate the bulk temperature of the system. This thermal difference between the nanoparticle surface and the surrounding medium can be leveraged to decouple bulk and surface phenomena, offering unprecedented control over nanoscale thermal stimuli. For instance, optical or luminescent thermometry techniques have revealed surface temperatures >60 °C higher than the surrounding solution, which can drastically affect adsorbed molecules, enzyme activity, or interfacial reaction rates, even under apparently mild conditions.[19]

Importantly, beyond this localized heating, MH can also enable efficient volumetric heating of the surrounding medium when desired. By adjusting key parameters (*e.g.* such as nanoparticle concentration, dispersion state, and AMF amplitude) it is possible to tune the thermal profile from confined nanoscale heating to homogeneous macroscopic temperature increases. At low nanoparticle concentrations, particles are typically well-dispersed and act independently, producing hot-spots scattered throughout the medium. These conditions are ideal for applications requiring precise, site-specific activation with minimal impact on the bulk temperature. Conversely, at higher concentrations, interparticle interactions and thermal overlap become more pronounced, allowing for more uniform and efficient heating of the entire medium.[31]

2.2 What governs heat generation in MH systems?

The heat released by MNPs under an AMF originates from their magnetic relaxation dynamics, which governs how their magnetic moments respond to the oscillating field. Two main mechanisms contribute to this process: Néel relaxation, involving internal reorientation of the magnetic moment within the nanoparticle core, and Brownian relaxation, driven by the physical rotation of the entire particle within the surrounding fluid. When the frequency of the applied field exceeds the characteristic relaxation time of the system, the magnetic moments cannot follow the field instantaneously, resulting in a phase lag and hysteresis behaviour. The area of the resulting hysteresis loop represents the energy dissipated as heat during each field cycle, and its magnitude depends on both the dominant relaxation pathway and the dynamic response of the system.

In fluid environments, such as aqueous suspensions or low viscosity organic media, both mechanisms may contribute simultaneously. The relative dominance depends on particle size, magnetic anisotropy, hydrodynamic volume, and the viscosity of the surrounding medium. For example, SPIONs with sizes around 10–15 nm tend to favor Néel relaxation, whereas larger particles with significant hydrodynamic diameters and low anisotropy may rely more heavily on Brownian rotation.[32] However, in immobilized systems, such as MNPs embedded in hydrogels,[33] grafted to polymer matrices,[34] confined within porous scaffolds,[35] or conjugated to biological targets (*e.g.* membrane receptors, enzymes, or antibodies),[36] Brownian motion is hindered or entirely suppressed. In these contexts, Néel relaxation becomes the primary mode of heat dissipation. This behaviour is particularly relevant in biomedical applications, where MNPs are internalized into cells or anchored to specific biomolecular targets. In such cases, optimizing the magnetic anisotropy and core size becomes critical to ensure efficient heating and no mechanical damage, especially under the moderate AMF conditions allowed for clinical use.

Beyond size and surface chemistry, other structural parameters strongly affect the heating performance. Shape anisotropy, for instance, can be exploited through nanocubes,[37] nanoflowers,[38,39] rods, or discs,[40] which alter the energy landscape for magnetization reversal. Internal defects introduce magnetic heterogeneities that increase energy dissipation under AMF cycling. Controlled defect engineering has been shown to significantly enhance heating efficiencies in various systems.[41,42]

Chemical composition is another powerful design lever. Doping iron oxides with elements such as zinc, manganese or cobalt enables tuning of the magnetocrystalline anisotropy and saturation magnetization, tailoring the relaxation dynamics to the AMF conditions. For instance, cobalt increases anisotropy and performs better under strong excitation.[43–45] In non-biological systems, high-magnetization metallic alloys like FeCo[46] or FeNi[47] can achieve much higher heating efficiencies, although their use is often limited by stability and toxicity concerns.

Ultimately, another important aspect of MNPs is their characteristic Curie temperature (T_c), or the temperature at which long-range spin ordering breaks down (transitioning from ferro/ferrimagnetism to paramagnetism)[48] due to thermal agitation overcoming such magnetic ordering. Thus, at temperatures near T_c, the magnetic susceptibility of MNPs dramatically drops, significantly impacting their ability to generate heat under an AMF. In this sense, MNPs with a T_c close to the desired operating temperature can offer self-regulating heating, minimizing the risk of overheating. However, heating efficiency declines due to the reduced magnetic response, potentially limiting the efficacy of the MNPs at that temperature. While this strategy has been studied for cancer therapy applications,[49] the engineering of MNPs with a tuned T_c for non-cancer applications is rare. All in all, we can say that the heating power of MNPs is reduced with increasing temperature because of the reduction of the area of the hysteresis loop and it becomes zero at the T_c.

In summary, the heating efficiency and therapeutic outcome of MNPs under AMF strongly depend on particle properties such as size, composition, and doping, as well as the frequency and amplitude of the applied field. For instance, MNPs in the 20–30 nm range exhibit high specific loss power under AMFs around 1 MHz and 5 kA m^{-1}, while larger particles can form magnetic vortices that enhance heating at similar frequencies.

Therefore, adjustments in AMF parameters are necessary to further modulate outcomes: increasing frequency favors Néel relaxation in smaller nanoparticles, enhancing localized heating, while higher field amplitudes increase temperature but must remain within safety limits.[50] Combined optimization of particle size, doping, and AMF conditions allows for controlled hyperthermia, targeted drug release, or enzyme activation. For example, advanced studies have shown tunable magnetic heating by adjusting these parameters in doped MNPs, offering precise thermal control for biomedical applications.[51]

Taken together, these design variables must be co-optimized depending on the intended application, considering not only the AMF parameters and medium properties but also the spatial localization and mobility constraints of the particles. Heating performance emerges from the interplay of all these factors and understanding that synergy is central to rational MH design.

2.3 What are the practical limitations of MH across different applications?

Despite its versatility, MH faces several practical limitations that are highly dependent on the target application. In biomedical contexts, the primary challenge is ensuring patient safety. High-frequency and high-amplitude AMFs can induce non-specific heating through eddy currents in conductive tissues. To mitigate this, safety guidelines, such as the Atkinson–Brezovich criterion, which limits the product of field amplitude and frequency ($H{\cdot}f$) to 4.85×10^8 A m^{-1} s^{-1}, are typically enforced. This restricts clinical use to frequencies of 100–300 kHz and field amplitudes below 15 kA m^{-1}.[52]

These limitations pose design challenges where MNPs must achieve efficient heating within a narrow AMF window,

especially in environments where Brownian motion is suppressed, such as intracellular compartments. Under such conditions, Néel relaxation dominates, which is generally efficient at higher frequencies (300–500 kHz), whereas Brownian relaxation tends to operate more effectively at lower frequencies (100–200 kHz) in fluid media.[53] Consequently, fine-tuning of the particle size, anisotropy, and relaxation dynamics becomes essential to match the system's relaxation time to the available field conditions and ensure adequate heat generation.

In contrast, non-biomedical applications (*e.g.* magnetically assisted catalysis) are not subject to physiological safety thresholds and can employ stronger and higher-frequency fields. However, they present a different set of limitations rooted in the thermal and physical properties of the surrounding medium. For instance, in organic solvents like mesitylene ($C_p \approx 1.7$ J g^{-1} K^{-1}) or in gaseous environments like air ($C_p \approx 1.0$ J g^{-1} K^{-1}), the combination of low heat capacity and low thermal conductivity allows for faster local temperature increases and limited heat diffusion.[54] This occurs because less energy is required to raise the temperature of mesitylene by 1 °C compared to water ($C_p \approx 4.18$ J g^{-1} K^{-1}), and heat is less efficiently dispersed throughout the medium, avoiding its dissipation. As a result, hot spots generated by MNPs are more easily sustained, enabling localized thermal activation and enhanced catalytic efficiency in confined or non-aqueous systems.

Yet, this thermal confinement also introduces practical drawbacks. Temperature monitoring becomes more difficult, as conventional thermometry may fail to capture nanoscale heat gradients, leading to underestimation of peak temperatures and the risk of overheating or thermal degradation. Non-uniform heating can result in inhomogeneous reaction kinetics, particularly during scale-up. Additionally, nanoparticle stability is a concern in reactive, high-temperature, or oxidative media, where aggregation or surface degradation may compromise heating efficiency. Finally, operating at high AMF intensities requires sophisticated coil engineering and thermal control, particularly in continuous-flow or large-scale systems.

In both biomedical and non-biomedical scenarios, effective implementation of MH depends on the precise coordination of nanoparticle design, field parameters, and environmental conditions. While the challenges differ across applications, the common requirement is a holistic, systems-level approach that integrates magnetic, thermal, and engineering considerations to harness the full potential of localized magnetic heating.

2.4 Is it possible to standardize the evaluation of MH performance?

Quantifying the heating efficiency of MNPs is essential for comparing materials and optimizing performance across different applications. The most widely used metric is the SLP or SAR, used very extensively in the literature. While useful, SLP is highly dependent on experimental conditions (particularly field amplitude, frequency, nanoparticle concentration, and thermal boundary conditions), making direct comparisons between studies difficult.[55] *In situ* magnetic field calibration using reference standards, strict control of sample stability, and harmonized protocols is recommended, otherwise SAR/SLP values from different groups are not directly comparable.[5] To address this, the intrinsic loss power (ILP) was introduced as a normalized parameter intended to decouple material performance from field parameters. ILP is defined as:

$$\mathrm{ILP} = \frac{\mathrm{SLP}}{f \times H^2}$$

expressed in nHm^2 kg^{-1}, where H is the magnetic field amplitude (A m^{-1}) and f is the frequency (Hz). Although ILP provides a convenient way to compare materials under different AMF conditions, it relies on the assumption of a linear magnetic response, which holds only for superparamagnetic particles under low-field conditions. In many practical scenarios, especially at high field amplitudes or with larger and more anisotropic particles, non-linear effects and hysteresis losses become dominant, rendering ILP inaccurate or misleading.[56] This limitation stems from the theoretical foundation of ILP, which is based on the linear response theory (LRT). LRT describes power dissipation in MNPs under the assumption that magnetization follows the applied field sinusoidally with a phase lag dictated by relaxation dynamics. While the model is valid in the low-field, superparamagnetic regime, its predictions deviate significantly in systems exhibiting hystereses or interparticle interactions, which are common in concentrated or aggregated samples.[55]

Determining the SAR/SLP or ILP value is generally achieved by analyzing the initial slope of the temperature variation against time plot when the AC field is switched on.[6] However, data analysis is also complex, resulting in great uncertainties associated with the final SAR/SLP/ILP value. Consequently, although SAR and ILP remain valuable tools, they should be interpreted with caution. Interestingly, in order to go one step forward in the standardization of this analysis, recent works have proposed alternative methods to extract that SAR/SLP value from the peak that arises in the on/off switching of the AMF.[4]

In summary, for reliable performance comparisons, standardized protocols are essential: precise reporting of field parameters, sample environment, and heat loss corrections. Moreover, alternative metrics based on hysteresis loop integration, frequency-dependent calorimetry, or AC magnetometry are increasingly employed to provide complementary insights into the dynamic magnetic behavior of MNPs beyond the assumptions of linear models.

3. Biomedical applications using magnetic hyperthermia beyond classical treatment

MH is being used in the development of biomedical applications not related to cancer treatment. A description of different applications together with selected examples is pro-

vided in what follows. A summary of different magnetic systems in terms of nanoparticle composition and size, and AMF conditions used in different biomedical applications can be found in Tables 1 and 2.

3.1. Drug delivery

In many clinical procedures, it is essential to control drug administration by carefully controlling the effective dosage, the time frame of drug application or the kinetics of drug release. However, as drugs are typically administered systemically, it is difficult to sustain effective drug concentrations over time due to limited control over diffusion rates. In addition, many drugs are poorly water-soluble and have short half-lives. These factors, along with the risk of systemic toxicity from exceeding the therapeutic dose, contribute to the harmful side effects often associated with pharmaceuticals. To address these challenges while maintaining efficacy, researchers are designing different drug delivery vehicles that, responding to an external stimulus, can release drugs at the desired dose with spatio-temporal control.

The main strategies using these thermo-responsive materials are based on heat-induced material transformation. However, other alternatives propose complete degradation of the thermoresponsive material (Fig. 1).

MH is used as an external stimulus to trigger the on-demand release of drugs for therapeutic purposes. Although these approaches have been widely explored in the frame of drugs for cancer treatment,[84,85] other alternatives for different molecules, such as antibiotics or anti-inflammatory drugs have been reported in the literature (see Table 1).

Regarding the use of thermoresponsive polymers, several approaches have been proposed, as the magnetic nanoparticles can either be coated with or embedded within these thermoresponsive polymers (Fig. 2). For example, thermoresponsive hydrogels for the storage and on-demand release of drugs using MH have been proposed using poly(*N*-isopropylacrylamide) (PNIPAM)[86] and poloxamer,[87] among others.

These materials undergo a phase transition from hydrophilic to hydrophobic states in response to temperature changes. By encapsulating magnetic nanoparticles within these hydrogels, the swelling and de-swelling behavior of the polymeric network can be precisely controlled by AMFs allowing the release of drugs.[88] This behavior has been tested for vitamin B_{12} delivery. This vitamin was released from the matrix of thermoresponsive hydrogels that contained MNPs when exposed to an external magnetic field. In addition to vitamin B_{12}, the release of methylene blue was also tested using these hydrogels. The application of pulsed AMF (5.3 kA m^{-1}, 297 kHz) for 5 min every 2 h showed effective modulation of methylene blue and vitamin B_{12} release.[86]

Another design approach is based on the generation of polymeric microspheres where both magnetic nanoparticles and drugs are encapsulated. Upon exposure to an external magnetic field, the permeability of the polymer matrix could increase, resulting in rapid drug release. This approach has been tested as an antibiotic release system using MH. Chitosan microbeads crosslinked with poly(ethylene glycol) (PEG) dimethyl methacrylate, loaded with vancomycin and iron oxide nanoparticles were tested. The nanoparticles were stimulated with an AMF for 30 min on days 3, 5 and 7 of the study. As a result, the daily elution rate of the drug increased up to 45% presumably due to

Table 1 List of non-cancer selected biomedical non-cancer applications of MH based on drug delivery

Drug type	Drug name	Hydrophilic/ hydrophobic	Delivery platform	Magnetic material	Size (nm)	H (kA m^{-1})	f (kHz)	Ref.
Antibiotics	Vancomycin	Hydrophilic	Thermoresponsive microspheres	Fe_3O_4	11	19.9	109.9	Mohapatra *et al.*[57]
Antibiotics	Vancomycin	Hydrophilic	Thermoresponsive microspheres	Fe_3O_4	11	8–20	110–525	Harris *et al.*[58]
Antibiotics	Amoxicillin	Hydrophilic	Magnetic core–SiO_2 shell nanoparticles	$Mn_{0.3}Fe_{2.7}O_4$	22	14 to 33	380	Wu *et al.*[59]
Antibiotics	Rifampicin	Hydrophobic	Magnetic nanocomposite scaffold	Mg_2SiO_4–$CoFe_2O_4$	30–100 nm	8, 10, 12 and 16	200	Bigham *et al.*[60]
Antibiotics	Erythromycin	Amphiphilic	Magnetoliposomes	Not reported	Not reported	4 and 12	100	Salah *et al.*[61]
Anti-inflammatory	Ibuprofen	Hydrophobic	Magnetic core–SiO_2 shell nanoparticles	Fe_3O_4	9	32	307	García *et al.*[62]
Anti-inflammatory	Diclofenac	Hydrophobic	Polymeric matrix	$CoFe_2O_4$	9	14.9	420	de Santana *et al.*[63]
Anti-inflammatory	Celecoxib	Hydrophobic	Polymeric matrix	Fe_3O_4	12–20	11	589	Ansari *et al.*[64]
Anti-inflammatory	Quercetin	Amphiphilic	Nanoparticles coated with polymers	Fe_3O_4	80–140 (8–12 nm cores)	9	50 and 100	Mandić *et al.*[65]
Coagulation factor	Thrombin	Hydrophilic	Thermoresponsive microspheres	Fe_3O_4	205 (7–10 nm cores)	30	100–513	Wang *et al.*[66]
Analgesic	Capsaicin	Hydrophobic	Nanoparticles coated with polymers	Fe_3O_4	25	22	250	Santi *et al.*[67]

Table 2 List of other non-cancer biomedical applications of MH

Biomedical application	MNPs system	Size (nm)	H (kA m^{-1})	f (kHz)	Ref.
Treatment of vascular diseases	Fe_3O_4	13	14.5	595	Liu *et al.*[23]
Organ rewarming and transplantation	Fe_3O_4	10	15	375	Wang *et al.*[68]
	Fe_3O_4	10	31.9	108, 163, or 208	Wakabayashi *et al.*[69]
	Fe_3O_4	10	63	180	Han *et al.*[70]
	Fe_3O_4	13	42.4	278	Chiu-Lam *et al.*[71]
	Fe_3O_4	Not reported	35	230	Chen *et al.*[72]
Treatment of bacterial infections	$MnFe_2O_4$	150 & 200 (~10 nm cores)	1.36	Not reported	Luo *et al.*[73]
	Fe_3O_4–ZnO nanocomposite	200–800 (~10 nm cores)	34	250	Singh *et al.*[74]
	Fe_3O_4	64 × 57	6.9	80	Chen *et al.*[21]
	Fe_3O_4	100 (10–13 nm cores)	18, 24 and 30	2100	Alumutairi *et al.*[75]
	Fe_3O_4	34	22	140	Jabalera *et al.*[76]
Food preservation	Fe_3O_4	10	34	873	Bañobre-López *et al.*[77]
Manipulation of cell membranes/signals	$MnFe_2O_4$	6	0.7	40 000	Huang *et al.*[78]
Cell transfection	Fe_3O_4	13	16.9	425	Idiago-López *et al.*[79]
Deep brain stimulation	Fe_3O_4	22	15	500	Chen *et al.*[80]
	Co-ferrite core/Mn-ferrite shell	8	15	500	Munshi *et al.*[81]
Sensors	γ-Fe_2O_3	12	29.4	180	Horny *et al.*[82]
Nanorobots	Fe_3O_4	6	15.9	100	Lopez *et al.*[83]

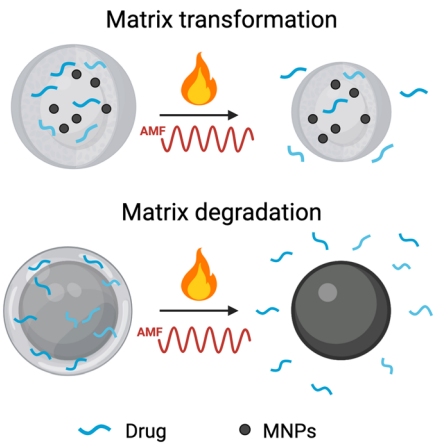

Fig. 1 Schematic illustration showing different nanoplatforms that enable the use of MH in the frame of on-demand release of drugs for therapeutic purposes. Each scheme represents the action occurring when heat is produced during exposure of the nanoplatform to an AMF. (Top) Matrix transformation, where heat is used to alter the nanoplatform structure and release the drug. (Bottom) Matrix degradation, where heat destroys the matrix with drug embedded and releases it. Figure created in Biorender.

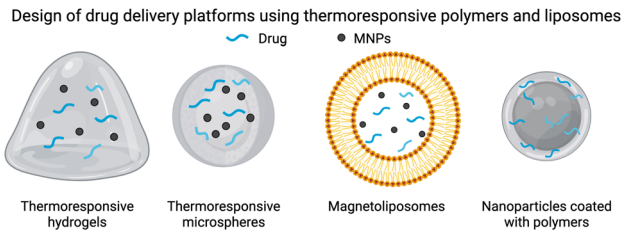

Fig. 2 Schematic illustration showing different drug delivery platforms (from left to right): thermoresponsive hydrogels,[86] thermoresponsive microspheres,[57] magnetoliposomes and nanoparticles coated with polymers.[61] Figure created in Biorender.

increased permeability in the beads. The study demonstrated that vancomycin was released for up to 8 days.[58]

Additionally, a similar system, with chitosan microbeads loaded with vancomycin, was tested by exposing the material to the AMF three times separated by 1.5 h. This different treatment resulted in a 200% higher release of vancomycin in the sample exposed to the AMF compared to the control.[57]

Nanoplatforms based on liposomes are another design broadly used in drug release using AMF experiments. These are commonly known as magnetoliposomes, which are spherical vesicles composed of one or more phospholipid bilayers enclosing MNPs (Fig. 2). Liposomes are structures formed from natural or synthetic phospholipids, which are amphiphilic molecules that naturally arrange themselves to prevent their apolar regions from interacting with water in an aqueous environment, leading to a double-walled hollow sphere with an aqueous core. Liposomes possess several properties that make them ideal for drug delivery. They are highly biocompatible due to the low reactivity of lipids, and their spatial conformation facilitates the encapsulation of both hydrophobic and hydrophilic therapeutic agents. Thanks to these benefits, liposomes were the first nanostructured drug delivery systems approved by the FDA for human use. In magnetoliposomes, drug release at the target site can be triggered by the heating

properties of MNPs when exposed to an AMF, thus improving the therapeutic efficiency.[61]

Magnetoliposomes can alter their structure and permeability, enabling controlled drug release. This permeability shift is linked to the melting temperature (T_m) of the lipid bilayer, which undergoes a phase transition from a gel to a fluid state, facilitating drug diffusion. Lipids with a T_m above physiological temperature (37 °C) are essential to prevent premature drug release.[61] Though liposomes with a higher T_m may slow down drug release, efficient MNP loading and heating can compensate for this. For example, dipalmitoylphosphatidylcholine (DPPC), with a T_m of 41.5 °C, is commonly used in thermoresponsive liposomes due to its proximity to clinically relevant hyperthermia temperatures. Surface grafting with polymers like PEG is an alternative that allows for fine-tuning of the phase transition and creates more versatile liposomal formulations.[61] Nevertheless, temperature-driven lipid phase transitions are not the only mechanisms for drug release. It was proposed that nanoparticle motion within the core could alter bilayer permeability and promote drug release in the presence of low-frequency AMFs.[89] On the other hand, it was described that bilayer-decorated magnetoliposomes that exhibited stimuli-responsive release properties showed that radio frequency heating induced both permeabilization and partial disruption of the bilayer.[90] Also, further works demonstrated drug release from core-loaded magnetoliposomes using short magnetic pulses, which caused mechanical motion of the MNPs without significantly increasing the local temperature. This motion generated ultrasound waves that destabilized the bilayer and facilitated drug release.[91]

Mild hyperthermia (42 °C) was also used to test the induced release efficacy of ciprofloxacin using low temperature-sensitive liposomes (LTSLs). *Staphylococcus aureus* plankton and biofilms were used for this purpose. This work also studied the feasibility of localized administration of ciprofloxacin in combination with hyperthermia delivery using magnetic resonance imaging (MRI)-guided high-intensity focused ultrasound (MR-HIFU) in a rat model. The results suggested that prolonged treatment might affect the biofilm matrix and deform the bacterial membrane, resulting in reduced survival rates.[92]

Alternative systems have been developed using thermally responsive materials that decompose under magnetic hyperthermia. Such materials are mainly used as coatings of MNPs that subsequently release molecules incorporated within them,[93] acting as drug delivery systems. One of the limitations of this approach, which has been discussed in the past, is the need for very high temperatures for their degradation that are both not feasible *in vivo* and may damage the structure of the attached drug. Interestingly, more recently, a different design, in which the temperature for coating degradation is feasible *in vivo* has been proposed. MH was used to melt the phase change material coating (a mixture of oleic acid and 1-hexadecanol) of MNPs and release the loaded drug, in this case thrombin, a drug used to treat aneurysms. In this case, the phase change material presented a melting point of 42.5 °C, which was also very interesting as it avoided higher temperatures that could denature the encapsulated drug.[66] Finally, in another recent example, MNPs were coated with a thermoresponsive polymer (poly(oligo(ethylene glycol) methyl ether methacrylate) (POEGMA)), which served as a capsaicin reservoir. When the particles were exposed to the AMF, capsaicin was released and used to regulate the pain receptor TRPV1.[67]

3.2. Treatment of vascular diseases

Each year, a large number of patients are affected by vascular diseases. These conditions, which affect the blood vessels and limit blood circulation, are major contributors to mortality rates globally.[94] In some of these diseases, heat produced by the MNPs using AMFs as an external stimuli can be used either as a treatment, to reduce some of the problems causing the diseases, or to slow down their advancement.

One example is the treatment of atherosclerosis. Atherosclerosis is characterized by the accumulation of lipids, cholesterol, and other substances on the arterial walls. This accumulation, known as plaque, can result in the narrowing of the arteries, obstructing blood flow. The rupture of plaque can then result in the formation of a thrombus, leading to a high risk of vascular occlusion. The accumulation of macrophages within the vascular wall is also a typical characteristic of atherosclerosis.[95] This fact, combined with the tendency of iron oxide nanoparticles to be phagocytosed by macrophages in the bloodstream, enables the particles to be accumulated at inflammatory sites, such as atherosclerotic plaques.[96] Therefore, several approaches have targeted atherosclerosis plaque through the accumulation of MNPs in macrophages.

For example, Fe_3S_4 nanoparticles were used to generate heat, using as stimuli a combination of AMFs and NIR light (photothermal treatment, PTT), to reduce the number of macrophages infiltrated in the arteries of a mouse model of atherosclerosis. As a result, the thickness of the carotid artery was reduced compared to the control group.[23] An additional complication in the progression of atherosclerosis arises from issues that can occur following the implantation of metallic stents. Restenosis is the re-narrowing of an artery that has previously been treated to reduce obstruction, for example after the placement of a stent. This re-narrowing leads to a recurrence of restricted blood flow. A completely different way of producing heat for the treatment of restenosis was developed based on the application of AMF, but using the stainless-steel stent as an antenna, instead of the typically used MNPs.[97]

3.3. Organ and cell rewarming after cryopreservation

Nowadays transplant medicine is considered one of the most promising fields in biomedicine with a noticeable impact on the life expectancy and quality of life of recipient patients. Solid organ transplantation has progressed from experimental to a definitive treatment for organ failure, incorporating organs like the liver, kidney, and heart.[98] Even though great advances in organ transplantation have been implemented, such as preservation, surgical techniques and immunosuppression, leading to higher survival rates and reduced compli-

cations, there is still room for development to continue improving all the processes associated with organ transplantation.

In this sense, MH provides a new experimental tool to allow the controlled heating of cryopreserved tissues and organs.[99] The approach of using MH for tissue rewarming is based on the perfusion of MNPs within the tissue during the cryopreservation steps (Fig. 3). When the cryopreserved organ is exposed to an AMF, particles produce heat, increasing the tissue temperature more homogeneously than if an external heat source is used.[69] Compared to classical methods such as microwaves, high frequency or infrared lasers, the MH has a more uniform distribution of heat exposure, does not involve a time-consuming process and does not need sophisticated instrumentation, which supports the idea of it being feasible for the rewarming of biological material.[100]

One example of this application was the development of a method for warming up human umbilical cord matrix mesenchymal stem cells (hUCM-MSCs). These cells exhibit interesting properties such as low immunogenicity and as a consequence a low incidence of graft rejection and post-transplant infection, which makes them attractive for regenerative medicine, but their recovery after cryopreservation is complex and challenging. The authors developed a strategy to generate a fast-heating rate using AMF and 10 nm MNPs that enabled the high efficiency recovery of hUCM-MSCs after cryopreservation. This novel method reduced the incidence of devitrification and/or recrystallization and in parallel increased the survival of rewarmed cells.[68]

The application of MH was also used for the rewarming of cryopreserved pancreatic islets, responsible for insulin production, before transplantation. In this work, the authors demonstrated a more uniform and rapid rewarming of vitrified islets using MNPs and AMFs, compared to gold standard convective warming using a 37 °C water bath. Such islets, obtained through magnetic heating, were also successfully transplanted into diabetic mice where the biological activity was preserved, reducing serum glucose levels.[69]

Whole organs were also rewarmed using magnetic heating after long-term cryopreservation in biological banks. Exposure of vitrified kidneys, previously incubated with nanoparticles, to an AMF allowed both rapid and homogeneous warming. These rewarmed kidneys were successfully recovered and after transplantation were able to restore full renal function in male rat model recipients.[70]

Another example of organs that have been studied for cryogenic storage using MH are hearts. In a theoretical approach, computational tools were used to evaluate the rewarming process in both human and rat heart models. They predicted that the anatomy and homogeneous distribution of MNPs inside hearts were crucial to reach the critical rewarming rate to avoid damage resulting from exposure to cryoprotective toxicity agents (CPA), which could also be relevant for the optimization of preservation protocols for this organ.[101] From an experimental point of view, a CPA that contained MNPs was developed. Particles remained stable in the cryopreservation agent VS55, both before and after vitrification and nanowarming. Besides, it was found that MNPs exhibited low cytotoxicity to primary cardiomyocytes. When whole rat hearts were perfused to remove the MNPs, magnetic particle imaging confirmed minimal residual iron in the hearts. All these observations indicated the suitability of the particles for perfusion, vitrification, and nanowarming of whole organs.[71]

Another interesting example was the procedure to rewarm articular cartilages. These tissues present some specific difficulties for cryopreservation/rewarming procedures because they have a very limited warming rate. This difficulty reduces their clinical potential despite increasing demand for clinical receptors. To address this issue, an ice-free cryopreservation technique was developed specifically for preserving large, intact, articular cartilage. Using AMFs (35.2 kA m^{-1}, 230 kHz) and MNPs, they achieved a rapid heating rate of 77 °C min^{-1}, which was several times faster than the traditional convection warming rate of around 5 °C min^{-1}. After cell and tissue analysis, the authors demonstrated the superior efficacy of their new approach for maintaining the structural integrity of large cartilage. Their findings revealed a depth-dependent preservation pattern, which was further validated using magnetic resonance imaging and computational modelling.[72]

Recently, similar approaches have also been applied to ovarian tissues. Improving the long-term storage of cryopreserved ovarian tissue is crucial to extend the fertility window of patients with fertility problems. In a recent study, the authors used PEGylated silica-coated MNPs to reduce injury in cryopreserved ovarian tissue from sheep. In particular, MH was implemented by adding nanoparticles to the vitrification media used to cryopreserve ovarian cortex fragments from a sheep model. To warm the cryopreserved tissues, the cryovials were placed in an AMF for 1 min. The tissue fragments were then cultured for eight days and compared to the conventional ovarian tissue cryopreservation method. The analysis showed that, compared to traditional warming methods, MH enhanced follicular development and gene expression, while reducing cellular apoptosis and oxidative stress, which made it an improved and feasible method for ovary tissue recovery after cryopreservation.[102]

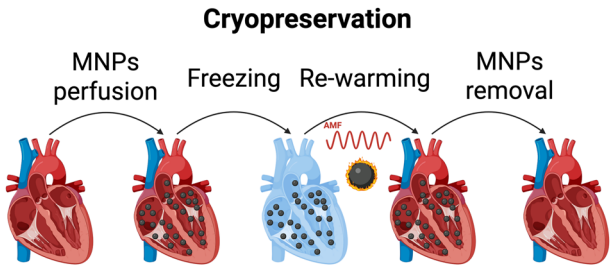

Fig. 3 Schematic illustration showing the steps for tissue cryopreservation and rewarming using MH. The particles must be perfused in the tissue before cryopreservation. Then, when the cryopreserved tissue is exposed to the AMF, heat released by the particles enables homogeneous rewarming of the organ. Figure created in Biorender.

Interestingly, for organ rewarming and cryopreservation, very similar conditions regarding particle size and composition and field amplitude and frequency were used in all the cases mentioned (Table 2), leaving room for further developments exploring other alternatives in the future. For example, as the particles are quickly removed after rewarming, maybe a broader MNP composition could be tested, given that the toxicity associated with particle degradation will not be a limiting factor, as in other biomedical applications.

3.4. Treatment of bacterial infections

Besides organ and cell rewarming after cryopreservation, the emergence of antibiotic-resistant pathogens represents a global health issue that needs urgent solutions. A recent study estimated 4.95 million deaths associated with bacterial antimicrobial resistance in 2019.[103] This number can increase as a consequence of resistance phenomena that arise from antibiotic administration. One innovative therapeutic strategy to treat bacterial infections is through the application of MH (Fig. 4), which enhances the bacteriotoxic and bacteriostatic effects of currently available antibiotics. An example of this approach is the combination of standard antibiotics with MH for the treatment of *Staphylococcus aureus* (*S. aureus*) infections.

The study found that MH by itself had little effect on killing *Staphylococcus aureus*, which is a common cause of chronic wound infections. Antibiotics like ciprofloxacin and vancomycin, while effective against free-floating bacteria, were not very effective against bacteria in biofilms. However, when biofilms were treated with MH for just 6 min, using 100 nm commercial Fe_3O_4 nanoparticles, the antibiotics worked much better. This effect was a result of the increased penetration of antibiotics through the biofilms after MH treatment.[75]

In the frame of wound healing, a synergistic strategy for biofilm treatments was also developed. In this recent study, the authors presented a therapeutic strategy combining quorum sensing (QS), a cell-to-cell communication mechanism used by bacteria, interference-assisted therapy with enhanced thermal treatment and immunomodulation in a single nanoplatform. In their approach, hyaluronic acid-coated ferrite nanoparticles were used as MH agents, disrupting QS-related genes and weakening the biofilm. This allowed deeper nanoparticle penetration, bacterial elimination through heat, and tissue healing triggered by bacterial enzymes. After analysis of *in vitro* and *in vivo* experiments, the results showed strong antibiofilm and anti-inflammatory effects, as detected by a reduction in TNF-α, IL-1b, and IL-6 proinflammatory mediators, which enhanced the effectiveness of traditional therapies.[73]

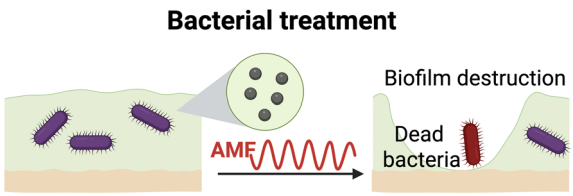

Fig. 4 Schematic representation showing the use of MH for bacterial treatments. Heat can be used for biofilm destruction, to kill bacteria or both. Figure created in Biorender.

Another study analyzed the use of superparamagnetic Fe_3O_4 embedded porous ZnO nanocomposite against both Gram-positive *Staphylococcus aureus* and Gram-negative *Escherichia coli* (*E. coli*) bacteria. Interestingly, exposure of Fe_3O_4–ZnO nanocomposites to AMFs for 1 h resulted in enhanced antibacterial activity compared to conventional heating methods used as controls, despite reaching equivalent temperatures during MH treatment (75 °C for Fe_3O_4 particles and 55 °C for Fe_3O_4–ZnO nanocomposites). The combined effects of hyperthermia, producing heat and generating reactive oxygen species (ROS), contributed to enhanced reduction efficacy.[74] A similar synergy of MH and ROS generation was observed with manganese–iron oxide nanoparticles ($Mn_xFe_{3-x}O_4$) acting as nanoheaters. In the *Hydra vulgaris* regenerative model, MNPs with a low Mn^{2+} content enhanced regeneration under magnetothermal stimulation, whereas MNPs with a high Mn^{2+} content caused a redox imbalance and impaired regenerative dynamics. These findings highlight a versatile strategy to manipulate ROS and redox homeostasis, with promising applications in both antimicrobial treatments and tissue engineering.[104]

An interesting novel approach for eradicating bacterial infections involves the use of *Magnetococcus massalia* strain MO-1 that could potentially kill pathogenic bacteria when applying an AMF.[105] These magnetotactic bacteria contain magnetosomes, which are unique organelles composed of single-domain magnetite (Fe_3O_4) or greigite (Fe_3S_4) nanocrystals coated by a membrane. A mixture of magnetotactic MO-1 strain bacteria and *S. aureus* was exposed to an AMF and standard viability assays were performed. Approximately 30% of the *S. aureus* cells were killed after the treatment. A higher *S. aureus* death (50%) after the magnetic treatment was observed if the magnetotactic bacteria were attached to *S. aureus via* specific antibodies. These results were also confirmed in mouse models, where MH using antibody-coated magnetotactic bacteria significantly enhanced wound healing. These results showed the eradication of *S. aureus in vitro* and *in vivo*, highlighting the potential of magnetotactic bacterium-mediated MH as a treatment for *S. aureus* in skin or wound infections.[21]

Also, in the frame of bacterial infections, MH has also been used to create an antibacterial therapy that delivers drugs directly to the infection site. A nanoformulation consisting of magnetic nanoparticles functionalized with the antimicrobial peptide AS-48 was evaluated against both Gram-positive and Gram-negative bacteria, both alone and in combination with MH. In that work, the application of MH demonstrated effectiveness specifically against *Pseudomonas aeruginosa* and *Klebsiella pneumoniae*, enhancing the sensitivity of resistant bacteria to the bactericidal effects of AS-48. This way, the application of MH not only makes localised infection treatment

possible but also could reduce and concentrate antimicrobial dosages. Furthermore, it will also enable mitigating secondary effects, including resistance development.[76]

Additionally, MH has also been explored in the frame of food spoilage caused by microorganisms. Magnetite nanoparticles were added to *Pseudomonas fluorescens*, and exposed to an AMF (100 Oe, 873 kHz). This treatment increased the temperature from 35 °C to 55 °C, resulting in the total eradication of the microorganisms in relatively short times (approximately 8 min).[77]

Together, these results support the idea that MH can serve as a complementary non-resistance-inducing mechanism for bacterial eradication, not only in biomedicine but also in novel food preservation technologies.

3.5. Manipulation of cell membranes and cell signals

The cell membrane is the biological barrier that surrounds and protects the cell, separating its internal environment from the external surroundings. This barrier is also responsible for the control of the in and out movement of substances within the cell, allowing selective transport of nutrients, ions, and waste. Several approaches have been developed in the past few years, including both the manipulation of membranes for the activation of cell functions in the frame of magnetogenetics and the manipulation of cell membranes for controlled drug delivery through bypassing traditional uptake pathways (Fig. 5).

Recently, many different tools were developed to manipulate cellular functions remotely. The main idea behind this approach is that cells have several receptors capable of sensing different physical cues from the environment and transforming that into cellular functions. Having this type of technology that enables the remote manipulation of these cellular functions is useful to shed light on our understanding of biological processes and to develop novel clinical applications. One of the stimuli being used in this scenario is magnetic nanoparticles located close to thermosensitive receptors that are exposed to AMFs (Fig. 5A).[106]

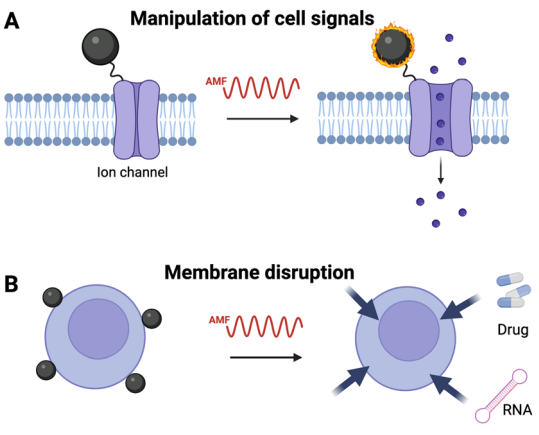

Fig. 5 Schematic illustration showing how MH can be used for cell membrane manipulation. (A) For cell membrane channel opening, the particles must be linked to the thermoresponsive cell receptor. Once the AMF is applied, heat produced by the particles opens the channel, allowing ion influx into the cell. (B) Particle linked directly to the cell membrane can change the permeability of the membrane, allowing drugs or small biomolecules to enter and avoid classical uptake routes. Figure created in Biorender.

The most studied thermoresponsive receptor is the TRPV1 channel, also known as the capsaicin receptor. TRPV1 is expressed in nerve cells and mediates several pathways such as glial function, cytokine secretion, plasticity and synaptic transmission. This receptor has a tetrameric structure and forms a pore that allows Ca^{2+} transport. This channel is activated at temperatures above ~40 °C.[107,108] As TRPV1 is expressed in nerve cells, one of the most explored applications of stimulation using magnetothermal stimulation is neuronal activation. For example, TRPV1 channels were activated using 6 nm $MnFe_2O_4$ particles exposed to an AMF. Among other experiments, they were able to demonstrate *in vivo* a significantly different behavioural response in *Caenorhabditis elegans* worms. When the magnetic field was applied, the amphid area of the nervous system could be heated specifically, reaching up to 34 °C, and the worms retracted despite being partially anaesthetized, leading to a thermal avoidance reaction in these animals.[78]

Using a different material (22 nm magnetite nanoparticles) and AMF conditions, TRPV1 was activated in deep brain neurons of mice brains. This study targeted the ventral tegmental area for magnetothermal stimulation by delivering TRPV1 to neurons in that area *via* a lentiviral vector, followed by the injection of magnetic nanoparticles. After exposing mice to an AMF, neuronal activation was measured through *c-fos* gene expression near the MNP injection site and results showed significant neural activation only in the group treated with both TRPV1 and MNPs. Control tests showed no activation with individual components, and activation closely aligned with TRPV1 expression, demonstrating an effective targeted magnetothermal stimulation.[80]

Furthermore, core–shell (12.9 nm, Co/Mn ferrites) particles were used to activate different brain areas that controlled the motor behaviour of mice using an AMF. With this approach, they were able to activate different motor responses of the animals while they were awake. In particular, three different responses, fast movement, rotational movement or motion inhibitory response, could be activated, depending on the areas of the brain that were activated.[81]

An alternative application being studied using the TRPV1 channel besides neuronal stimulation is the remote regulation of protein expression. Using 20 nm iron oxide nanoparticles and exposure to an AMF, the synthesis of insulin *in vivo* was stimulated in mice. The treatment was able to reduce blood glucose levels in mice receiving this treatment.[109]

Additionally, from the same family of cation channels, the TRPV4 channel can also be activated by increased temperature (among other stimuli, such as hypotonicity or acidic pH). TRPV4, as TRPV1, also has a tetrameric structure with a pore that allows Ca^{2+} transport. The expression of this channel has also been reported in cells of the central and peripheral

nervous system, but also in other organ systems such as the eye, ear, heart, digestive, respiratory, urinary, and reproductive systems among others.[110]

Moreover, although less studied, another ion channel that has been tested for its thermal activation using MH is the temperature gated chloride channel anoctamin 1 (TMEM16A). This channel has been studied using Co–Mn–ferrite nanoparticle core–shell particles in rat hippocampal neuronal cultures transfected to express TMEM16A and exposed to AMFs. Upon field exposure, they were able to silence neuronal activity.[81]

In all the research works described to date, synthetic magnetic nanoparticles were used as heat generators; however, this approach requires that the particles are administered to the animals and reach the specific cells that have to be activated. Alternatively, other works have made use of biogenic magnetic nanoparticles through the generation of ferritin nanoparticles. Ferritin is the iron storage protein that can accumulate biomineral iron in its inner cavity. Using ferritin linked to TRPV1 channels, *in vivo* insulin gene expression was modulated when mice were exposed to AMFs.[111] With the same approach they were also able to activate glucose-sensing neurons.[112] Nevertheless, the use of ferritin for channel activation remains controversial.[113]

All these results highlight the potential of using MH in the frame of neuromodulation and can open access to therapeutic opportunities for different cell therapy approaches in the future.

In addition to the manipulation of cell signals, being able to modulate the cell membrane is also interesting to enable the introduction of therapeutic agents directly into the cell, bypassing traditional pathways like endocytosis and avoiding endosomal entrapment (Fig. 5B). This can enhance the efficiency of drug delivery, particularly for large or cell-impermeant molecules. For example, MH was recently used to disrupt the plasma membrane in living cells using heat. The idea relies on the attachment of MNPs to the cell membrane *via* bioorthogonal click chemistry. While the particles are in the membrane, the AMF is applied, producing local heat that enables the internalization of cell-impermeant probes. Interestingly, this thermal stimulus does not induce cell death. This approach was used for transfecting cells with small interfering RNA, opening the way for the direct intracellular delivery of biomolecules or other relevant species, bypassing traditional endocytosis pathways.[79]

In addition to living cells, MH has also been used to modulate membranes in the frame of synthetic cells. In the frame of synthetic biology, researchers are producing synthetic cell models that allow us to understand specific processes occurring within living cells. These synthetic cells also allow for the design of customized pathways for targeted applications such as microreactors for bioproduction. Very recently, synthetic magnetoresponsive organelles were generated using thermoresponsive membranes coupled to MNPs. They embedded such organelles within synthetic cells to generate a bioreactor for enzymatic catalysis.[114]

For this type of approach, one of the key aspects for successful application is to be able to control the location of the particles in the biological system, either near the iron channels or on the cell surface. Therefore, complex functionalization of the MNPs is required.

3.6. Sensors

In the context of early diagnosis, reducing timescales and improving sensitivity and specificity are key parameters for the development of new assays. Some sensors are based on amplification processes of biological targets by catalytic reactions where heating is a required critical step. However, in microfluidic devices, excessive heating must be avoided, as high temperatures can lead to the denaturation of chip components. Recently, local heat production in the frame of MH using nanoparticles was used to develop lab-on-chip systems that avoided global sample heating. DNA-modified superparamagnetic core–shell nanoparticles were able to capture complementary sequences (such as microRNA targets). MH was then used to release these targets locally for further detection by electrochemistry.[82]

Given the limited number of published works on this topic, the possibility of using MNPs with complex compositions (as no toxicity limitations are required) and the possible use of small AMF applicators using a wider range of field amplitudes and frequencies opens the way for the fast and easy development of this underexplored application.

3.7. Nanorobots and MH for biomedical applications

Over the past two decades, research has increasingly focused on the development of magnetic nanorobots. These nanorobots are generally described as nanoparticles containing magnetic materials such as iron oxides (Fe_3O_4), engineered to perform several tasks (Fig. 6). For example, loading mobile nanodevices with therapeutic cargo, such as drugs or biological molecules, that are released through remote manipulation using external magnetic fields offers a high degree of spatiotemporal control.[115,116] State-of-the-art developments in the design and fabrication of micro- and nanorobots, the mechanisms that drive their propulsion, advanced imaging techniques, safety considerations, and their diverse applications were recently reviewed.[117]

The exposure of nanorobots to AMFs can be used to generate different responses. One of the possibilities that magnetic nanorobots offer is the activation of some functions through heat generation when exposed to AMFs, converting energy from AMFs into heat, leading to tissue ablation or destroying cells while sparing healthy tissue. Additionally, exposure to AMFs can induce oscillatory or rotational motion in nanorobots by creating magnetic torque or gradient forces on their magnetic components, for example, guiding nanorobots through complex biological environments, such as blood vessels or tissues and enabling penetration into dense tissues or biofilms. Moreover, exposure to AMFs may also produce mechanical responses by the magnetic nanorobots, for

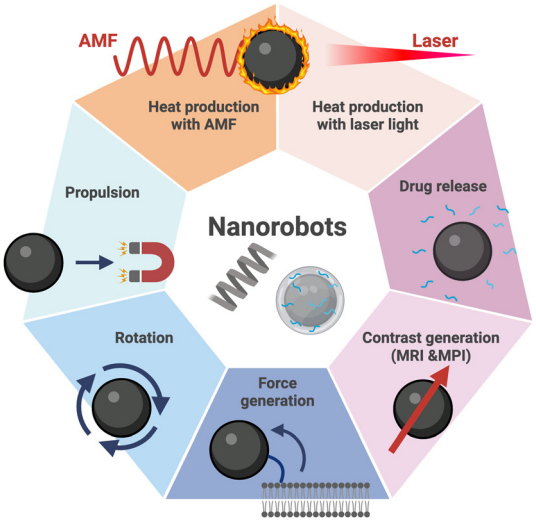

Fig. 6 Nanorobots are nanoparticles that can perform several tasks, which in the case of magnetic nanoparticles include movement guided by magnetic fields, heat production and other specific activities such as drug delivery or contrast generation in imaging techniques. Figure created in Biorender.

example, assisting in thrombolysis and ischemia mitigation through clot dissolution.

Some examples of recent advantages combining magnetic nanorobots and AMFs include their use for intracranial aneurysm therapy without stents or microcatheters. These nanorobots, guided by magnetic fields (3–4 Hz, 15 mT) and ultrasound, released thrombin to quickly occlude an aneurysm through localized MH. The results showed complete, safe, and stable embolization after two weeks, paving the way for less invasive and more effective therapies.[66]

Another example of magnetic nanorobots was their loading with an enzyme (nattokinase) used for thrombosis treatment. They combined mechanical propulsion using low frequency magnetic fields (15 Hz, 0–260 mT) and enhanced MH triggered by high-frequency fields (375 kHz, 33 mT) to release the enzyme and dissolve clots. The treatment achieved 81% recanalization of vessels in thrombosis mouse models. This dual-frequency magnetic system holds great potential for targeted thrombolytic therapies.[118]

Magnetic fields can penetrate deeply into biological tissues, making this method effective for *in vivo* applications, particularly in areas like the brain. For example, nanorobots were also proposed to swim in cerebrospinal fluid for non-invasive brain therapy with the aim of generating personalized dynamic drug delivery to the brains of mice to treat brain tumors.[119] Additionally, MNPs exposed to AMFs were tested in rat brain capillaries; these transiently and reversibly increased blood–brain barrier permeability without causing inflammation.[120]

These approaches have great potential for treating brain diseases such as strokes and Parkinson's disease.

By coupling AMFs with nanorobots, researchers are achieving unparalleled precision and versatility in targeted therapies, opening new frontiers in nanomedicine, and manipulating nanorobots in inaccessible regions, such as the brain or dense organs, reducing the need for surgical interventions. Optimization of this therapy needs a balance of AMF intensity and frequency to maximize efficacy while avoiding tissue damage. In addition, it would be interesting to combine AMFs with imaging techniques (*e.g.*, magnetic resonance imaging (MRI), magnetic particle imaging (MPI), ultrasound, and magneto-photoacoustic imaging) for real-time tracking and guidance and developing robust AMF systems and nanorobots for clinical applications.

4. Non-biomedical applications of magnetic hyperthermia

MH has also emerged as a powerful tool in non-biomedical applications, providing a unique approach for catalysis and environment applications. A description of different applications together with selected examples is provided in what follows.

4.1. Catalysis applications

AMF mediated catalysis (sometimes called "induction heating") generally relies on a local temperature rise to increase the rate of a chemical reaction.[121] When heat is applied, the energy of the reactant molecules increases, making it easier for them to overcome the energy barrier of the reaction.

As stressed in section 2.1 (What makes MH fundamentally different from conventional heating?), conventional heating often leads to significant energy loss, uneven heating, and slower reaction rates, especially in large-scale systems. Hyperthermia-based heating, by contrast, is a selective process that focuses energy directly on the MNPs (that may be the catalyst) or near the reaction site, achieving faster and more efficient temperature elevation at these crucial points. This targeted approach allows for more precise control over reaction conditions, ensuring that the catalyst remains at an optimal temperature for activation without unnecessarily heating the surrounding environment. This focused energy input not only enhances reaction rates but also enables higher selectivity in multi-step reactions, as specific reaction pathways can be activated or suppressed by precisely controlling the localized temperature.[19] Consequently, hyperthermia-based heating offers both energy efficiency and improved control over reaction dynamics. The energy-efficient nature of hyperthermic catalysis holds the potential to reduce operational costs.[122] Since the hyperthermic process targets only specific zones or surfaces for heating, it consumes less energy overall compared to traditional bulk heating methods, which heat the entire reaction vessel. This efficiency is especially valuable for industrial-scale processes, where energy consumption can be a major operational cost.

Moreover, enhanced reaction rates due to localized heating mean that reactions can reach completion faster, which

reduces both processing time and energy requirements per cycle. Collectively, these benefits position hyperthermia-based approaches as a sustainable and economically attractive option for industries looking to implement more cost-effective and environmentally responsible catalytic processes.

Fig. 7 summarizes different processes that were shown to be catalysed by MNPs thanks to hyperthermia-based heating.

Among different possible reactions, MH catalysis has been used for many different reactions including fine chemical synthesis, flow process intensification, high-temperature endothermic catalytic processes and high-temperature exothermic catalytic processes.[122] It is worth noting that MNPs can act as both heating agents and catalysts, or be employed in combination with a catalyst with high catalytic activity for a specific reaction. In the frame of MH mediated catalysis, heterogeneous catalysis, in which the phase of the catalyst or substrate (*e.g.*, MNPs) differs from that of the reagent or product, is most reported in the literature.[123] Finally, catalysts and reactor designs have evolved to integrate this technology in processes able to store intermittent energies.[124] Table 3 summarizes different catalytic reactions, the efficiency of which was enhanced through MH and some selected examples.

4.1.1. Advanced synthesis processes. MH has been used for fine chemical synthesis and flow process intensification. Probably, the first example of MH mediated catalysis involved using silica coated Fe_3O_4/Fe_2O_3 NPs, modified with catalytically active palladium, as catalysts for the synthesis of organic molecules. The reactions reported were transesterifications, condensation reactions (to form thiazoles), Claisen rearrangements and catalytic transformations such as the Buchwald–Hartwig amination of aryl bromide and enyne metathesis to yield dihydrofuran. Their induction system accommodated a flowthrough reactor filled with superparamagnetic material. Indeed, Fig. 8A shows that hyperthermia heating (flow reactor heating) is much faster in comparison with conventional heating (for conventional heating, the reactor was heated in an oil bath).

Fig. 8B shows typical yields of isolated products in three different reactions when using either conventional heating (batch reactor) or a flow reactor (inductively heated). In all cases, yields are 10–30% higher when inductive heating is used.[17] Typically, the flow reactor is loaded with MNPs. The reactor could operate up to a backup pressure of 5 bar. Importantly, after the reaction mixture passes through this type of reactor, the system must be flushed with an appropriate solvent (methanol, ethanol, ethyl acetate, toluene, *etc.*).

Other catalysed processes aided by inductive heating in continuous flow employed silica coated MNPs decorated with catalytically active gold, demonstrating the successful oxidation of allylic and benzylic alcohols to aldehydes and ketones, using oxygen gas or atmospheric air.[125]

MH has been used for catalytic processes occurring at very high temperatures. For example, highly endothermic reactions that require temperatures as high as 800–900 °C, such as steam reforming or steam methane reforming (SMR), can be performed using MH. In particular, alloys of cobalt and nickel (cobalt and nickel weight percentages were in the range of 0–13% and $MgAl_2O_4$ was the support) were used for SMR and the use of MH allowed sufficient power input to be produced to equilibrate the reaction at above 780 °C with more than 98% conversion of methane.[126] This could consequently enable a more compact steam reformer design. Another example to achieve high temperatures is the use of $Fe_{0.5}Co_{0.5}$ particles, which can be used as universal heating agents, allowing reactions to be performed up to *ca.* 700 °C upon association with the appropriate catalyst. Some interesting reactions that were performed using this approach were CO_2 hydrogenation, dry reforming of propane and methane, and dehydrogenation of propane, which required temperatures of 350 °C, 600 °C, and 700 °C, respectively.[13] Dry reforming of methane and propane were carried out in the presence of a nickel NP catalyst, whereas dehydrogenation of propane required PtSn NPs as a catalyst. In these cases, in which very high temperatures are reached, the catalyst needs to have a Curie temperature that is at least as high as the operating temperature. Most elements cannot maintain a magnetic moment on their own at temperatures above 100 °C. Of pure elements, only nickel, iron and cobalt can be used at elevated temperatures, with Curie temperatures of 354, 770, and 1115 °C, respectively. Notably, cobalt readily oxidizes under the high temperatures and water partial pressures of the SMR process, making it challenging to prevent the formation of antiferro- and paramagnetic phases.[136] Alloying with nickel provides a dual solution to this as nickel is an excellent catalyst for the endothermic SMR and nickel stabilizes the cobalt phase against oxidation while maintaining activities like that of pure nickel. In line with this, magnetically induced CO_2 methanation was shown for different MNP compositions, including core–shell NPs consisting of nickel or ruthenium coated iron carbide cores, NiCo alloy NPs, iron oxide NPs and NiFe alloy NPs.

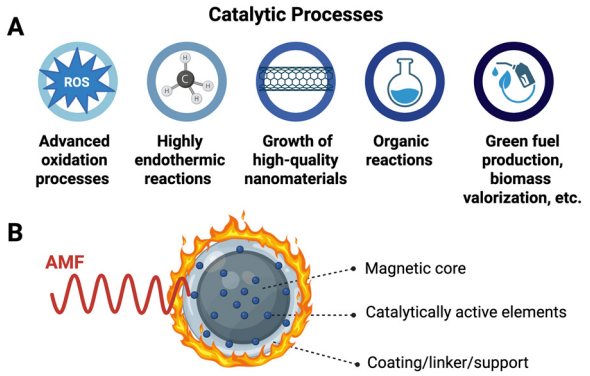

Fig. 7 (A) Catalytic processes involving the use of magnetic nanoparticles (MNPs) and MH heating: including organic reactions, highly endothermic reactions such as steam methane reforming (SMR), growth of high-quality nanoparticles, advanced oxidation processes (AOPs), green fuel production and biomass valorization, among others. (B) The design of MNPs typically employed for catalytic applications includes a magnetic core that will act as a heating agent, some coater/linker/support and may include other catalytically active elements. Figure created in Biorender.

Table 3 List of non-biomedical applications of MH: MNP systems developed for catalytic processes

MNP system	Size (nm)	H (kA m^{-1})	f (kHz)	Catalytic process	Authors
Fe_3O_4/Fe_2O_3@SiO_2-Pd	10–40	Not reported	25	Advanced synthetic processes: organic reactions (transesterifications, condensation, Claisen rearrangements and Buchwald–Hartwig amination)	Ceylan *et al.*[17]
MAGSILICA®-Au	~20 (Au NPs 2–5)	Not reported	25	Advanced synthetic processes: organic reactions (oxidation of allylic and benzylic alcohols to aldehydes and ketones)	Chaudhuri *et al.*[125]
Co@$MgAl_2O_4$NiCo@$MgAl_2O_4$	11–24	32	68	Highly endothermic processes: steam reforming reaction (methane and steam are converted into hydrogen and carbon monoxide)	Mortensen *et al.*[126]
(Co@C and FeCo@C) FeCo@C : Co@C (2 : 1)–Ni/Pt–Sn	12–17	13–20	93–300	Highly endothermic processes: CO_2 methanation	Martínez-Prieto *et al.*[13]
$Fe_{30}Ni_{70}$–Ni@$SiRAlO_x$[b]	14–22	20	300	Highly endothermic processes: CO_2 methanation	De Masi *et al.*[127]
$Fe_{2.2}C$–Ni@$SiRAlO_x$	Ni: 2–3 $Fe_{2.2}C$: 14–15	13–64	93–300	Highly endothermic processes: CO_2 hydrogenation into methane	Kale *et al.*[128]
Fe_3O_4–Au	Fe_3O_4: 33 Au: 24	Not reported	110	Catalytic reduction reaction of resazurin to the fluorescent resorufin	Yassine *et al.*[14]
$CoFe_2O_4$	16–18[a]	Not reported	100	Decomposition of H_2O_2 and oxidation of caffeine	Tatarchuk *et al.*[129]
Fe_3O_4/Fe_2O_3	21	13–26	222	Adsorption/degradation process of methylene blue	Rivera *et al.*[130]
Fe_2O_3	40	8–40	100–200	AOP experiments for the degradation of organic compounds	Gallo-Cordova *et al.*[131]
Fe_2O_3	15–60	16	200	AOP experiments for the degradation of anionic (acid orange 8) and cationic (methylene blue) dyes	Gallo-Cordova *et al.*[132]
FeC–Ni	15	20–38	300	Electrocatalytic reactions relevant for water splitting	Niether *et al.*[133]
Fe_3O_4@Al_2O_3/KOH	18	48	100	Synthesis of fatty acid methyl esters (FAMEs), which constitute biodiesels	Corrales-Pérez *et al.*[18]
$FeNi_3$@Ni	16	37	93	Hydrodeoxygenation reaction (HDO) and cleavage of lignocellulose-derived products	Marin *et al.*[15]
NiCo	NiCo: 16	0–36	93–300	Hydrodeoxygenation reaction (HDO) and cleavage of lignocellulose-derived products	Mazarío *et al.*[16]
NiCo–Ru	Ru: 2				
$Fe_{2.2}C$–Ru	Ru: 3–4 $Fe_{2.2}C$: 14–15	46	300	Hydrodeoxygenation of biomass platform molecules	Asensio *et al.*[134]
FeCo@Ni	FeCo@Ni: 12	50–100	300	Reduction of biomass-derived	Cerezo-Navarrete *et al.*[135]
FeCo@Ni@C	C: 3			Oxygenated compounds	

[a] Average particle size was quantified by XRD. [b] Ru can be used as coating material but it reduces the yield of the reaction.

Among them, $Fe_{30}Ni_{70}$ alloy particles stood out, displaying high heating powers at low magnetic field amplitudes and achieving conversions of 100% and methane selectivity of 100%.[127] This is related to the fact that FeNi alloys display low anisotropy and a sufficient saturation magnetization, making this material a good candidate for reaching high temperatures under magnetic excitation at a low field amplitude. In addition, the authors highlighted that the spatial separation of the heating agent and the catalyst was important to obtain high yields. Another process catalysed by local heat generated by MNPs is the conversion of resazurin into fluorescent resorufin.[14] An important point to bear in mind is that nickel based catalysts are the most widely studied due to the best trade-off between activity and cost.[128] In addition, as we have seen above, ferromagnetic iron, cobalt, nickel and their alloy materials with precious metals (gold, platinum, palladium, *etc.*) represent some of the most popular compositions; these were shown to be catalytically active for chemical processes with high relevance for industry.[137]

Another interesting example of using MH in a catalytic process is the growth of high-quality graphene films, employing an inductively heating cold-wall reactor (heated by a catalytic copper substrate under the action of AMFs).[138] Such rapid temperature ramp up/down holds great potential for large scale and rapid manufacturing of graphene with much better energy efficiency. In addition, it was demonstrated that in solution, and under mild conditions of temperature and pressure, it was possible to use MH to carry out transformations that were otherwise performed heterogeneously (*e.g.*, after deposition of the heating agent and the catalyst on a support) at higher pressures and/or temperatures. Thanks to MH, the authors could use milder conditions of temperature (reactor temperature was *ca.* 165 °C; indeed, at the MNP surface, the temperature is higher) and pressure (3 bar of H_2) for this catalytic process. In particular, they could perform the hydrodeoxygenation of acetophenone derivatives and of biomass-derived molecules, namely furfural and hydroxymethylfurfural.[134]

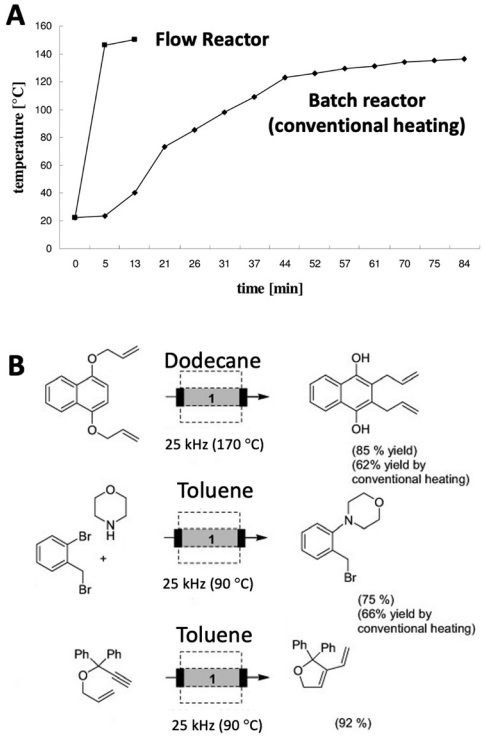

Fig. 8 (A) Heating profile of a batch reactor (oil bath with temperature control) in comparison with a flow reactor (inductively heated magnetic nanoparticles, 25 kHz, 340 per mille). (B) Selected chemical processes that were successfully catalysed with inductive heating mediated by MNPs. Yields of isolated products produced by either conventional heating (batch reactor) or in a flow reactor (inductively heated) are also shown. Adapted from ref. 17 with permission from John Wiley & Sons, Inc.

Such transformations are carried out industrially using high catalyst loadings, temperatures up to 280 °C and high pressures of H_2 (from 10 to 50 bar). Thus, the benefits of MH local heating for this catalytic process are clear.

It is worth noting that the successful use of MNPs as heating sources and catalysts or catalysts supports depends on some fundamental parameters:

- The intrinsic characteristics of the nanoparticles (size, shape, composition, *etc.*). Indeed, the effects of size and local heat on the catalytic efficiency are crucial: it is commonly expected that the efficiency of a nanoparticle catalyst increases with decreasing particle size because the binding energy to the smaller particles is higher.

- The temperature achieved on the particle surface. Indeed, the temperature near the nanoparticle surface can be even more important than that of the medium, especially when physical contact is necessary. In this sense, inorganic luminescent probes in direct contact with the particle surface revealed a much higher temperature (64 °C more) on the particles' surface than the macroscopic temperature determined by means of standard fibre-optic probes.[139] In addition, the coating of the MNPs plays an important role. This is because heat dissipation can be reduced depending on the surface of the catalyst, for example the presence of ligands like oleic acid, tetramethylammonium hydroxide, *etc.*[140] It was demonstrated that the treatment of MNPs with pyridine led to the removal of ligands, which had a profound implication for the induction heating catalyzed oxidation reaction of 1-octanol.

- MNP agglomeration and sintering (at high temperatures). This phenomenon can be circumvented by confining the MNPs in another material, such as carbon. This was the case for FeCo and cobalt NPs coated with carbon (Co@C and FeCo@C), which led to ultrastable heating agents suitable for high-temperature magnetically induced catalysis.[13]

- The MNPs' magnetic properties. For example, cobalt is a hard magnetic material with a high magnetocrystalline anisotropy and a high Curie temperature (T_c > 1000 °C), which would require very high field amplitudes at room temperature to release heat. On the other hand, iron oxides are soft magnetic materials with much lower magnetocrystalline anisotropy and T_c, needing much lower field amplitudes to release heat. As such, depending on the catalytic process, the combination of hard and soft magnetic materials may be interesting, either in a single hybrid nano-object (leading to a material that can be activated at lower magnetic amplitudes) or by simple mixing (without interacting directly). This enables, upon magnetic excitation, pre-heating of the hard material through the heat released by the soft material. This would in turn decrease the coercivity of the hard material and render magnetic heating by the hard heating agent possible. In fact, the combination of cobalt and FeC NPs with Ni-based catalysts showed excellent catalytic performances for magnetically induced CO_2 methanation (90% of CO_2 and 100% CH_4 selectivity, even at a very low field, namely 16 mT and small amounts of catalysts). In addition, as cobalt has a T_c surpassing 1000 °C, this combined material is a promising catalyst for chemical reactions requiring high temperatures such as methane reforming.[128]

It is worth mentioning that the influence of magnetism on catalytic reactions remains largely unexplored and not thoroughly established. Previous research on magnetic catalysis has primarily focused on electronic properties,[141] structural attributes, or the interactions between molecules and magnetic catalysts through electron transfer. These interactions can significantly alter magnetic properties and are themselves influenced by the application of an external magnetic field. Recent investigations involving Pt_3M alloy structures have demonstrated that spin–electron interactions in magnetic catalyst materials can contribute energetically to facilitate molecular chemisorption. Additionally, iron oxide-based ferromagnetic nanoparticle catalysts have been found to act as spin polarizers under strong magnetic fields, promoting spin-selective adsorption of oxygen species on catalyst surfaces during the oxygen evolution reaction, thereby aiding the formation of triplet-state O_2. These findings suggest that optimizing atomic ordering, even on the surface, and enhancing ferromagnetism within magnetic nanoparticle structures can significantly improve their catalytic performance.

Also, it has to be highlighted that compared to conventional reactors, induction-based ones require a higher level of com-

plexity. It was stated that the current readiness level of this technology was low; this means many scientific and technical issues have to be addressed before the question of cost-effectiveness can be examined.[142] In addition, few cases reported that AMF application decreased the enzymatic activity to around 50%.[143] All these matters must be solved and tackled in the future.

Finally, MH has also been explored in other catalytic applications with significant environmental impact. As seen in the next subsections, for instance, in advanced oxidation processes (AOPs), MNPs can serve as both catalysts and localized heat sources, accelerating the degradation of persistent organic pollutants. Finally, we show that MH has been applied in green fuel production, where the localized heating of magnetic catalysts enables more energy-efficient conversion of feedstocks into biofuels. In biomass valorization, the technique facilitates thermo-catalytic transformations by enhancing reaction rates and selectivity under milder bulk conditions.

4.1.2. Advanced oxidation processes. Over the past decade, AOPs have emerged as a leading solution for water and wastewater remediation, employing chemical treatment methods specifically designed to eliminate organic contaminants from aqueous effluents. These processes rely on the generation of highly reactive oxygen species like hydroxyl radicals ($^{\bullet}OH$), superoxide anions (O_2^{-}), and hydroperoxyl radicals ($^{\bullet}OOH$), among others, which are capable of oxidizing a wide range of pollutants, including those that are resistant to conventional treatments (Fig. 9). AOPs include techniques such as ozone-based oxidation, Fenton and Fenton-like reactions, photocatalytic processes, and electrochemical oxidation.

MH can significantly enhance these AOPs by integrating MNPs that act as both catalysts and localized heat sources under an AMF. This dual functionality can accelerate reaction rates, improve energy efficiency, and enable pollutant degradation under controlled conditions.

Within MH AOPs, ferrite nanocatalysts have proved to be excellent candidates for degrading organic pollutants due to their efficient magnetic heating properties. Cobalt ferrite nanocatalysts were used for the oxidation of caffeine. This work revealed an increase in oxidation efficiency from 40% to 85% under the exposure of an AFM. However, such a study did not analyze the temperature reached during the process, which is a critical parameter for hyperthermic applications.[129]

For hyperthermic processes, monitoring temperature variations is essential, as the enhanced efficiency may be attributed to localized heating at the nanocatalyst surface rather than bulk temperature changes. In controlled temperature environments, it is feasible to precisely investigate the sole effect of MH on AOPs. Iron oxide nanocatalysts were evaluated under controlled temperature conditions for their performance in the MH adsorption and degradation of methylene blue. To specifically evaluate the impact of magnetic hyperthermia on methylene blue degradation, experiments were designed where the reaction medium was conventionally preheated prior to the application of the AMF. The reaction itself commenced with the addition of H_2O_2 after the desired temperature was reached. Remarkably, reaction yields can be increased by 5% when the catalyst is exposed to an AMF.[130]

Extending these findings to other contaminants in real systems, MH-AOPs have demonstrated similar enhancements in reaction yields during the mineralization of solid landfill leachate and the textile industry effluents. Using iron oxide nanoflowers exposed to an AMF, mineralization efficiencies exceeding 80% were achieved. Notably, in this study, a reaction temperature of 90 °C was reached solely through MH, eliminating the need for conventional preheating. Nevertheless, the reaction was initiated only after achieving the required temperature.[131]

When considering MH, it is important to take full advantage of the temperature at the surface of the catalysts. Studies on the degradation of model compounds such as methylene blue and acid orange 8 have shown that preheating the medium is unnecessary to achieve high mineralization yields. This approach provides a significant advantage for industrial effluent treatment, particularly where discharge temperatures are typically below 30 °C, eliminating the need for costly cooling processes. By initiating the Fenton-like reaction simultaneously with the application of an alternating AMF, the reaction medium can reach just 35 °C after 1 h, but it achieves degradation efficiencies of up to 50%, demonstrating the energy-efficient potential of MH in wastewater treatment.[132] Moreover, in systems targeting emerging contaminants like microplastics, MH-AOPs have achieved mineralization yields of approximately 80%. This enhanced degradation was attributed to localized hot spots on the nanocatalyst surface and the generation of hydroperoxyl radicals, as confirmed by electron paramagnetic resonance (EPR) measurements.[144]

When dealing with this kind of Fenton-like system it is important to evaluate the ROS that nanocatalysts can produce

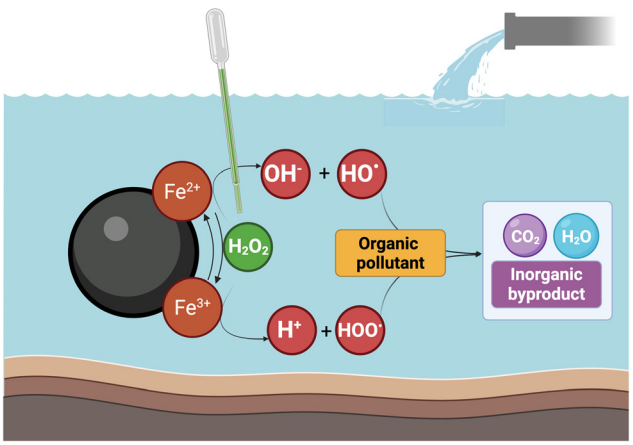

Fig. 9 Schematic representation of an advanced oxidation process (Fenton reaction). Magnetic nanoparticles (*e.g.*, Fe^{2+}/Fe^{3+}) catalyze the decomposition of hydrogen peroxide (H_2O_2) into reactive oxygen species such as hydroxyl radicals ($^{\bullet}OH$ and $HO_2^{\bullet}$), which degrade organic pollutants into harmless inorganic byproducts like CO_2 and H_2O. Figure created in Biorender.

in aqueous media. EPR spectroscopy is a widely used technique to measure ROS in various chemical and biological systems. EPR detects unpaired electrons in paramagnetic species, making it a powerful tool for directly identifying and quantifying short-lived radicals like hydroxyl radicals ($^{\bullet}OH$), superoxide anions ($O_2^{\bullet-}$), and other ROS.[145] In this sense, several authors working with AOPs focus their research on analysing ROS to determine the catalytic efficiency of their materials. For example, a cascade mechanism with alkoxyamine-grafted iron oxide nanoparticles that release radicals when exposed to AMF was described by following the reaction kinetics with EPR. This approach allowed for precise control over pollutant degradation, with localized heating triggering radical formation at lower energy inputs compared to conventional AOPs.[146]

Additional advancements in MH-AOPs can be achieved by employing materials with enhanced magnetic properties and improved ROS production. Fe-based metallic glass catalysts were used for this purpose, demonstrating exceptional recyclability and high degradation rates for organic dyes such as rhodamine B and methyl orange. The application of an AMF played a crucial role in regenerating Fe(II) and sustaining ROS production, allowing for up to 100 reuse cycles without significant loss of catalytic activity. The study attributed accelerated charge transfer for ROS regeneration to the Kelvin force, while the Lorentz force and high-frequency vibrations induced by the AMF facilitated O_2 bubble release. This mechanism exposed additional active sites on the nanocatalyst surface, further enhancing catalytic efficiency.[147]

4.1.3. Green fuel production. Green fuels are emerging as key solutions to global energy challenges due to their potential for zero-emission energy generation and storage. MH has been described as a tool for hydrogen and biodiesel production (Fig. 10). Hydrogen, produced *via* water electrolysis, is a promising alternative to fossil fuels, enabling cleaner transportation, industrial applications, and power generation. However, challenges such as high energy requirements and sluggish reaction kinetics hinder the efficiency of hydrogen production. Researchers are exploring innovative approaches for enhancing these processes, and one such promising method is the use of MH to improve efficiency and reduce energy consumption in hydrogen production.

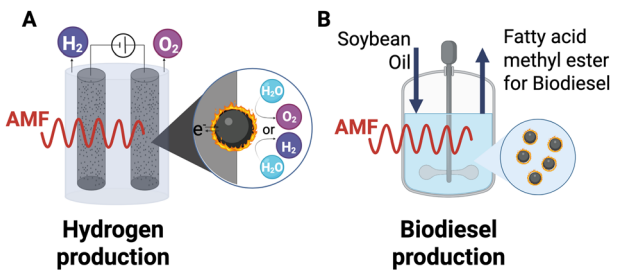

Fig. 10 Use of MH in green fuel production. (A) In hydrogen production, AMFs can activate magnetic catalysts, enhancing water electrolysis by locally increasing the reaction temperature and improving electron transfer. (B) In biodiesel production, AMF-induced heating of magnetic nanoparticles accelerates the transesterification of oils (*e.g.*, soybean oil) into fatty acid methyl esters, optimizing yield and energy efficiency. Figure created in Biorender.

Integrating magnetic nanoparticles with efficient heating capabilities into electrochemical systems can greatly enhance the efficiency of water splitting,[148] a crucial reaction for sustainable hydrogen fuel production. For instance, magnetic nanocatalysts can be engineered with core–shell structures, featuring a magnetic core such as iron carbide (FeC) and a nickel shell. Under an AMF, these systems have demonstrated exceptional heating performance with SARs up to 2000 W g^{-1}. Additionally, the nickel shell serves as an effective catalytic phase for electrochemical water splitting. When incorporated into the electrodes of an alkaline water electrolysis cell, these nanoparticles reduce the overpotential required for the oxygen evolution reaction (OER) by 200 mV and for the hydrogen evolution reaction (HER) by 100 mV. This enhancement is equivalent to raising the system's temperature to approximately 200 °C, despite an actual temperature increase of only about 5 °C, highlighting the highly efficient localized heating effect.[133] In addition to enhancing the HER and OER efficiency through temperature increase *via* MH, it is possible to achieve a higher current efficiency by thermally modifying the electrocatalyst. This modification, such as thermal expansion of the metallic electrode lattice, optimizes hydrogen adsorption and desorption, thereby improving the catalytic performance.

Recent research described the use of iron-coated nickel foam electrodes, which, when exposed to a high-frequency AMF, produced localized heating that significantly boosted both the HER and OER activity. Under intermittent induction cycles (60 s on, 60 s off), the method achieved a remarkable 540% increase in overall water-splitting current, with the HER current rising approximately sixfold at −1.4 V and the OER current increasing 1.8 times at 0.6 V, both measured at 20 mA cm^{-2}.[149]

Biodiesel, on the other hand, is a renewable and biodegradable fuel produced through the transesterification of triglycerides found in vegetable oils, animal fats, and waste cooking oils.

Biodiesel synthesis typically requires temperatures above 60 °C and a basic or acidic catalyst. Conventional homogeneous catalysts pose challenges in separation, recyclability, and cost, leading to interest in magnetic nanoparticles as an alternative.[150,151] Magnetic catalysts, including mixed metal oxides, supported catalysts, and metal–organic frameworks (MOFs), offer high surface areas, strong catalytic activity, and reusability, reducing costs and waste.[152,153] However, most studies fail to demonstrate the benefits of MH in biodiesel production. MNPs, acting as localized nanoheaters in hyperthermic processes could enhance reaction kinetics, lower energy consumption, and optimize conditions. Thus, developing nanocatalysts with improved heating capacity and basicity is key to increasing efficiency and sustainability.

In a recent study it was confirmed that incorporating iron oxide nanoparticles within an alumina matrix impregnated with KOH could provide both catalytic activity and efficient

heating under an AMF. The optimized system, operating with 5% catalyst loading, and a methanol-to-oil ratio of 12 : 1, achieved a biodiesel conversion of 98.6% and 95.6% yield, as confirmed through NMR characterization. The iron oxide nanoparticles exposed to the AMF raised the reaction medium temperature to 60 °C, ensuring efficient transesterification. The designed nanocatalyst demonstrated excellent magnetic reusability, although a slight decline in performance over multiple cycles was observed due to potassium leaching.[18]

These advancements, within green fuel production, highlight the promising role of MH in green fuel technologies, offering a novel method for improving the performance of both water electrolysis and transesterification processes, thereby contributing to the development of sustainable energy solutions.

4.1.4. Biomass valorization. Biomass stands out as a key renewable resource for the sustainable production of high-value-added chemicals. Recent research has explored innovative methods for enhancing biomass conversion efficiency, focusing on the use of magnetic nanoparticles and magnetic induction as advanced catalytic tools. By leveraging the advantages of MH, various biomass feedstocks, including lignocellulosic and sugar-derived materials, can be efficiently converted into valuable products through thermally enhanced catalytic pathways.[154]

MH proved to be highly effective at converting sugar-derived biomass intermediates, such as furfural and 5-hydroxymethylfurfural (HMF), into valuable biofuel precursors. Using bimetallic $FeNi_3$ nanoparticles enriched with nickel ($FeNi_3$@Ni) under a high-frequency AMF, the nanoparticles generate localized heat, raising the solvent temperature to 150–160 °C and significantly enhancing the catalytic activity. This targeted heating effect facilitates the complete conversion of furfural into 2-methylfuran and HMF into 2,5-dimethylfuran, both of which are high-energy-density biofuel precursors.[15]

In lignocellulosic biomass valorization, the selective cleavage of lignin's complex aromatic structure can be mediated by MH with NiCo and NiCo–Ru nanoparticles, by accelerating the cleavage of C–O bonds in lignin-derived compounds such as diphenyl ether (DPE), guaiacol, and vanillin. The synergy between nickel and cobalt, boosted by ruthenium, enhances the hydrodeoxygenation activity, achieving 77% conversion under an AMF, more than doubling the performance of conventional heating at 180 °C.[16] A notable feature of this process is the ability to control product selectivity by adjusting the magnetic field amplitude using core–shell FeCo@Ni, and carbon-coated FeCo@Ni@C MNPs, where the nickel shell provides catalytic activity, and the carbon coating enhances stability and recyclability. For example, in the conversion of HMF, applying 50 mT results in 100% selectivity for 2,5-bishydroxymethylfuran (BHMF), while increasing the field to 83 mT shifts the selectivity entirely to 2,5-dimethylfuran (DMF), a valuable biofuel.[135]

4.2. Environmental remediation

4.2.1. Soil remediation. MH holds promise for addressing various pollutants in soils, including organic compounds and heavy metals. By generating localized heat, it is possible to induce desorption of specific contaminants from soil and even degrade them into harmless products. For example, zero-valent iron nanoparticles in combination with an AMF proved to be effective at the remediation of volatile organic compounds like trichloroethylene (TCE) in soils. The heat generated by zero-valent iron nanoparticles under AMF can effectively enhance the desorption and degradation of TCE up to approximately 5 times compared to the absence of the AMF. Interestingly, the ferromagnetic properties of zero-valent iron nanoparticles allow them to produce significant thermal energy and increase contaminant mobility while accelerating the degradation reaction rate.[155]

Incorporating zero-valent iron nanoparticles into foam has the potential to effectively target contaminants located in specific sections of soil, such as the unsaturated areas within the vadose zone. In this case, foam can serve as a carrier vehicle to deliver zero-valent iron nanoparticles into the unsaturated porous media to efficiently evaporate TCE with MH. Specifically, the application of an AMF can facilitate the volatilization of TCE, achieving a temperature increase of up to 77 °C within 15 min. This resulted in a 40-fold increase in TCE volatilization compared to untreated conditions.[155]

An essential parameter to consider in the desorption of contaminants from soil is pH, as it significantly influences the properties of soil components involved in contaminant interactions. This parameter regulates the interactions between adsorbates and adsorbents during removal processes. At acidic pH values, the zero-valent iron surface is prone to corrosion, generating significant amounts of Fe(II) species. This corrosion process contributes to the preservation of metallic iron, enhancing its heating capacity under these conditions. The role of soil pH in the magnetic hyperthermic desorption of *m*-xylene using zero-valent iron nanoparticles was investigated. This study revealed that zero-valent iron could achieve temperatures exceeding 60 °C within 20 min under an AMF, reducing the residual *m*-xylene fraction by 86.4% within 1 h. Moreover, the researchers adjusted the pH using fulvic acid. At lower pH levels, fulvic acid exhibited electrostatic attraction to both zero-valent iron nanoparticles and *m*-xylene, facilitating closer contact between the heating source and the contaminant. This proximity improved thermal conduction, resulting in more effective desorption.[156]

Interestingly, it is possible to incorporate magnetic nanoparticles, which can serve to heat soil for the desorption of contaminants, into geotextiles. For example, citric acid-coated iron oxide nanoparticles can serve as heating agents in non-woven and woven polypropylene geotextiles. When placed in contaminated soils, the geotextiles can effectively generate and transfer heat to the surrounding soil under AMFs. This method can achieve rapid temperature increases of approximately 40 °C in less than 1 min in different soils like clay and sand, demonstrating its potential for efficient and localized soil remediation.[157]

4.2.2 Water treatment. Beside catalytic processes to eliminate pollutants from water like AOPs, there are other methods

to purify water that can fully take advantage of hyperthermia. Among these, membrane-based systems have attracted attention for their potential to integrate magnetic materials in innovative ways. By incorporating magnetic nanoparticles into filtration membranes, it becomes possible to use localized heating as a functional tool, enhancing cleaning efficiency and maintaining the performance without the use of harsh chemicals. Traditional filter membranes face challenges such as biofouling, which leads to operational interruptions and increased costs. To address this, it is possible to consider biofouling removal methods using membranes coated with magnetite nanoparticles.[158] By applying an AMF, the magnetic nanoparticles can rapidly heat the membrane surface to disintegrate biofoulants without compromising the membrane's filtration performance. Similarly, a study by Anvari *et al.* developed composite magnetic–hydrophilic/hydrophobic membranes by spraying iron oxide-coated carbon nanotubes (Fe-CNT) onto polytetrafluoroethylene membranes for an inductive heating vacuum membrane distillation system. Under the induction heating system, saline water on the membrane's surface was directly heated, optimizing permeate flux based on the Fe-CNT loading, conductive layer thickness, feed flow rate, and vacuum level.[159]

4.2.3. Air pollution control. Air pollution control, particularly the mitigation of carbon dioxide (CO_2) emissions, is a critical global challenge due to its profound impact on climate change and environmental degradation. CO_2, a major greenhouse gas, accounts for a significant portion of anthropogenic emissions, primarily from fossil fuel combustion and industrial activities. Effective strategies for CO_2 capture, storage, and utilization are essential for reducing atmospheric concentrations and achieving sustainability goals. Among these strategies, capture and desorption processes using advanced materials have emerged as promising solutions due to their efficiency and scalability. Recent advancements, such as the integration of MH into carbon capture systems, offer a transformative approach for enhancing these processes. By leveraging the localized heating capabilities of magnetic nanoparticles under AMFs, MH enables precise, energy-efficient regeneration of adsorbents primarily within magnetic induction swing adsorption (MISA).

Integrating magnetic nanoparticles like magnetite (Fe_3O_4) into metal–organic frameworks (MOFs) has enabled the development of magnetic framework composites (MFCs), which offer a highly effective solution for CO_2 desorption. One example of this approach involves the incorporation of Fe_3O_4 into N-doped porous carbon composites, which enhances CO_2 capture and energy efficiency. These systems allow for the rapid and uniform heating of adsorbents through a fixed target temperature, achieving high desorption rates with remarkable energy efficiency.[160]

By optimizing the Fe_3O_4 : MOF ratio, the efficiency of MISA has been shown to surpass conventional temperature swing adsorption techniques. Thermally treated composites, such as HKUST-1 containing Fe_3O_4 nanoparticles, demonstrate superior thermal responses under AMFs, achieving 93 °C. This facilitated efficient desorption and full regeneration of the material at approximately 130 °C, with desorption rates reaching 3.27 mg g^{-1} s^{-1} and complete CO_2 release. These composites can maintain structural integrity and adsorption–desorption performance over 20 cycles, highlighting their durability for industrial-scale CO_2 capture applications.[161]

Additional advancements in MISA technology demonstrated the potential for combining it with other targeted release techniques to enhance CO_2 desorption processes. A series of pioneering studies explored the incorporation of citric-acid-passivated MNPs into Mg-MOF-74, revealing that MFCs with a high magnetic nanoparticle content (7.76 wt%) achieved an excellent heating performance. Under an AMF, these composites reached a temperature increase of 41 °C within 20 min, enabling up to 67.3% CO_2 release at 0.35 bar in just 21 min.[162] Building on these results, subsequent research explored the synergistic effects of MISA and light-induced swing adsorption (LISA) using a family of metal–organic frameworks (MOFs) called PCN-250 (an iron-based porous coordination network) embedded with Fe_3O_4 nanoparticles. This dual-stimuli method, termed MaLISA (a combination of LISA and MISA), achieved desorption efficiencies of up to 96.8% while maintaining low energy consumption (Fig. 11).[163] It was also demonstrated that 100% CO_2 release could be achieved by subjecting MFCs to an AMF, with regeneration times as short as 240 s. These results underscored the critical role of MNPs in overcoming the thermal insulation challenges of MOFs, enabling rapid and uniform heating and further solidifying the potential of these advanced composites for energy-efficient CO_2 capture and desorption processes.[164]

4.3. Material transformations

By generating localized heat, hyperthermia can effectively influence characteristics such as viscosity, curing rates and phase transitions. This has been exploited in the frame of self-healing polymers, cement curation and oil viscosity reduction.

4.3.1 Self-healing polymers. The basic idea behind self-healing polymers is to build materials able to self-repair after damage. Several different self-healing processes were proposed and recently reviewed.[165] Interestingly, one of these approaches makes use of MNPs embedded in the polymer for the development of self-healing materials that recover their properties after exposure to an AMF. This idea is based on the fact that many self-healing polymers rely on the increased temperature for the repair process (see Fig. 12).

In healing processes that are based on an increased temperature, such as those activated by MH, it is important to determine the "healing window", a range of temperatures that go from the initiation of healing due to melting to the start of deformation processes when too high temperatures are reached.[166] To avoid reaching the deformation stage, some works have also explored the idea of using MNPs with a self-limiting heating behavior.[167] This approach, which avoids irreversible side reactions that occur at high temperatures, allows for several cycles of damage and repair.

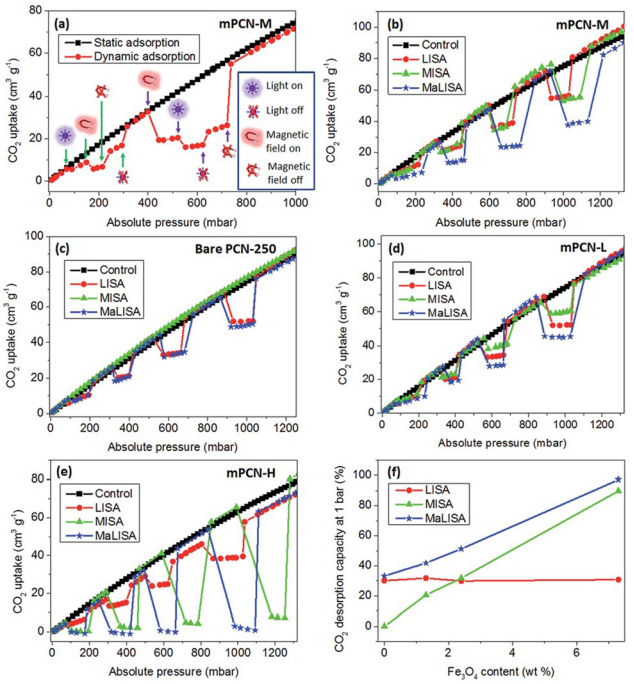

Fig. 11 Successive typical cycles of CO_2 take up and release using a metal–organic framework (MOF) called PCN-250 (an iron-based porous coordination network) with embedded magnetic nanoparticles. Magnetic PCN-250 (mPCN) was used with increasing MNP contents (L < M < H) ranging from 1.3 wt% (mPCN-L) and 2.4 wt% (mPCN-M) to 7.3 wt% (mPCN-H). Three excitation approaches were used: LISA (light-induced swing adsorption), MISA (magnetic induction swing adsorption) and MaLISA (a combination of LISA and MISA) processes. (a) Two successive typical switching cycles of CO_2 take up and release in mPCN-M through LISA, MISA and MaLISA processes. Dynamic switching of CO_2 capture and release in mPCN-M (b), bare PCN-250 (c), mPCN-L (d), and mPCN-H (e) by LISA, MISA and MaLISA processes. (f) CO_2 desorption capacities of mPCNs at 1 bar adapted from data shown in (b)–(e). All the dynamic CO_2 adsorption profiles were obtained by intermittently exposing the samples to 365 nm UV light (LISA process) and/or an alternating magnetic field of 17.6 mT and 279 kHz (MISA process) during CO_2 adsorption measurements at 298 K. Reproduced from ref. 163 with permission from the Royal Society of Chemistry.

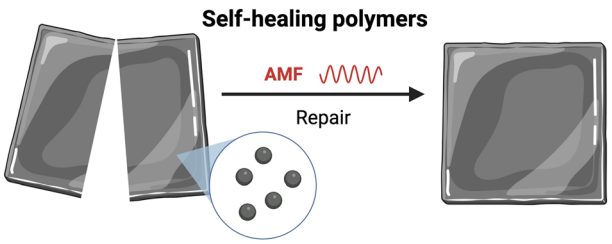

Fig. 12 Schematic illustration of the self-healing process for polymeric materials mediated by magnetic hyperthermia. Figure created in Biorender.

Self-healing polymers based on MH are mainly used to recover the mechanical and electrical properties of polymers. Regarding the recovery of mechanical properties, it was shown that polymeric films containing dispersed magnetite/maghemite nanoparticles could be cut, separated, attached to form a physical contact and exposed to an AMF to repair the cut. This treatment also results in mechanical strength retention even after repeated cut and repair cycles.[168] A similar approach was also used to validate the self-healing process of polymers that were subjected to chaffing and tear using Mn–Zn ferrites.[169]

Regarding the recovery of electrical properties, superparamagnetic nanoparticles added to thermoplastic polymers were used to repair areas of the material that were damaged by local electric fields.[170] When the material was exposed to an AMF, the heat produced by the particles enabled restoration of the polymer properties, in particular the dielectric strength and the electrical resistivity.

Besides their use in structural or electrical repairs mentioned earlier, this type of self-healing material is now being developed for a wide range of applications, including printable magnetoresistive sensors[171] or magnetic soft actuators[172] among others.

4.3.2 Cementation and oil mobilization. MH can be applied in cementation processes under extreme climatic conditions where it can be employed to facilitate curing (Fig. 13A). Specifically, silica-coated iron oxide nanoparticles act as heating agents, producing thermal energy through magnetic induction when exposed to an AMF. This targeted heating accelerates cement hydration, ensuring appropriate setting even in cold or humid environments where conventional methods often fail. The approach not only enhances curing efficiencies but also reduces energy consumption by eliminating the need for external heating systems, which are usually large in this kind of setting (*e.g.* in drilling sites for oil extraction).[173]

On the other hand, selective adsorption, long-range transport, localized heating, targeted tracking, and recovery are characteristics of MNPs that are highly advantageous for advanced applications in petroleum production.[174] In particular, MNPs under AMFs have been used to increase the temperature of petroleum to reduce its viscosity and facilitate its transportation (Fig. 13B). SAR was measured under different variables to determine its potential in the oil and gas (O&G) industry. The effects of colloidal stability, fluid viscosity, and NP concentration were studied for this application.[25] For example, employing 9 nm iron oxide MNPs coated with oleic acid under AMFs, allowed for the determination of SAR values in solvents with increasing viscosity (at 25 °C): diesel (4.7 mPa s), oleic acid (27.6 mPa s) or their mixtures with heavy (124.3 mPa s) or waxy (333.9 mPa s) crude oils (final MNP concentration was 0.5–1.0 wt%). SAR values were in the range of 25–225 W g^{-1} and the authors claimed that the Néel relaxation mechanism was dominant in the system. Besides O&G, other industries (pharmacy, the food industry, *etc.*) highlight that a reduction in viscosity can translate into lower costs and greater profitability.[175] In line with this, it was predicted, though not experimentally demonstrated, that by reaching a maximum of ΔT = 16.3 °C (using 1 wt% NPs), a decrease in the heavy crude oil viscosity of 45% would occur.[176]

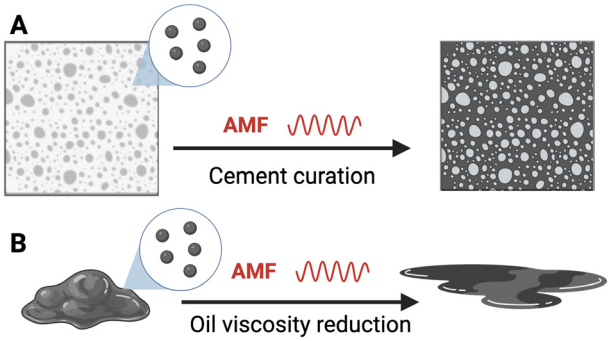

Fig. 13 Applications of magnetic hyperthermia in construction and oil processing. (A) AMF induces localized heating in magnetic particles embedded in cement mixtures, accelerating curing and enhancing material properties. (B) In oil processing, AMF exposure reduces oil viscosity *via* magnetic nanoparticle heating, improving flow and facilitating extraction or transport. Figure created in Biorender.

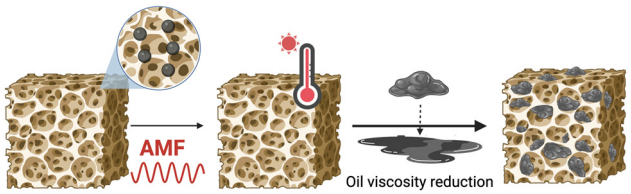

Fig. 14 Schematic illustration of the design required for enhanced oil recovery (EOR) methods using MNPs (also the so-called "ferrimagnetic sponge"). MH leads to efficient clean-up of viscous crude oil. Figure created in Biorender.

Another potential application where MH and MNPs are employed to reduce the viscosity, as previously explained, is in enhanced oil recovery (EOR) techniques, which are crucial for maximizing the extraction of residual oil from mature reservoirs.[177] This is because heavy crude oil is difficult to clean up due to its high viscosity and low fluidity, which prevent it from being easily absorbed by conventional porous sorbents. This makes the removal of heavy crude oil spills especially challenging.

To address this issue, the reduction in its viscosity thanks to the use of MNPs and MH has been explored. In this sense, ferrimagnetic sponges (see Fig. 14) with hydrophobic porous channels are shown to be promising materials. Their surface can be remotely heated to 120 °C within 10 s under an alternating magnetic field of f = 274 kHz and H = 30 kA m^{-1}.[178] Importantly, the authors could achieve a notable reduction of viscosity and continuous recovery of crude oil (33.05 g h^{-1} cm^{-2}) *via* remote magnetic heating. Thus, MH-assisted EOR methods using MNPs could offer promising advantages over conventional EOR methods such as steam injection and *in situ* combustion; however, critical aspects like efficiency and nanoparticle reusability remain still underexplored and should be addressed in future studies.

5. Discussion, trends and future perspectives

Traditionally used in cancer therapy, MH is expanding into several fields beyond oncology, revealing exciting possibilities in neuromodulation, tissue engineering, and environmental cleanup among others. These applications demand tailored MNP compositions and AMF conditions, with biocompatible iron oxides preferred for biomedical uses while diverse alloys can be used for industrial processes.

Indeed, non-biomedical uses of MH can leverage alternative nanomaterial designs—varying in size, chemical composition, and coatings—which may not necessarily require biocompatibility. Fields such as catalysis[13,126,134] and pollutant degradation[129] benefit from novel compositions incorporating transition metals, noble metals, and semimetals. These tailored designs enhance MH efficiency and optimize various processes, including catalytic reactions, formation and degradation mechanisms, heat and mass transfer, and material transportation. For catalytic applications, much more complicated nanostructures are used including different composites (Table 3). Additionally, in this type of application, higher temperatures, above 150 °C, can be reached by increasing the nanoparticle concentration and using stronger magnetic field intensities (>30 kA m^{-1}), which significantly improve the reaction efficiency in shorter times.[15]

For biomedical uses, in general, most studies rely on iron oxide nanoparticles with core sizes of about 10 nm, sometimes aggregated into 100–200 nm multicore structures (see Tables 1 and 2). For drug delivery, variable AMF fields of 10–30 kA m^{-1} and 100–600 kHz are often applied in short pulses (5 min) repeated several times after hours, reaching temperatures below 45 °C to avoid degradation of the encapsulated drugs (Table 1). However, complete eradication of bacterial pathogens[75] and the stimulation of specific cells *in vivo*[78] require AMF at higher thermal doses (MHz range) and a high local density of nanoparticles to achieve significant regional heating (Table 2).

The generation of reactive oxygen species during magnetic hyperthermia remains a critical limitation for biomedical applications. Excess ROS can damage healthy tissues by inducing oxidative stress, disrupting cellular membranes, and altering essential biomolecules.[179] While moderate ROS levels may contribute to therapeutic effects, such as antibacterial activity,[75] uncontrolled production raises safety concerns. Current strategies to mitigate this problem include optimizing nanoparticle coatings, controlling field intensity and exposure time, and combining magnetic hyperthermia with antioxidant delivery systems.[180] Understanding the balance between therapeutic and harmful ROS levels is therefore essential to advance the safe clinical translation of this technology.

An important strategy to improve the safety of magnetic hyperthermia is the use of nanoparticles with self-limiting heating properties.[181] These materials, often based on magnetic alloys or systems with well-defined Curie temperatures,

can restrict their maximum heating once a critical temperature is reached. This effect prevents an uncontrolled thermal increase, reducing the risk of damaging healthy tissues while maintaining sufficient heating for therapeutic purposes. Such self-regulation is particularly relevant for *in vivo* applications, where precise control of local temperature is difficult, but also for non-biomedical applications, like self-healing polymers,[167] in which too high temperatures can damage the material. By tailoring the composition and magnetic properties of the nanoparticles, it is possible to design systems that automatically stop heating above the desired therapeutic window, offering a promising approach for safer and more efficient biomedical treatments.

Finally, when designing magnetic hyperthermia experiments, the applied AMF should fit with the relaxation dynamics of the nanoparticles. Good practice is to characterize the effective relaxation time in the relevant medium and select a field frequency close to the calculated resonance. The field amplitude should be adjusted to enhance the heating efficiency but always within the accepted *H·f* safety limits in biomedical applications, to avoid non-specific tissue heating.[182] We recommend systematic validation of SAR under conditions that mimic the *in vivo* environment, including nanoparticle immobilization and realistic concentrations, to ensure both reproducibility and translational relevance.

In parallel, current AMF commercial applicators are designed with the constraints imposed by oncological and *in vivo* applications in mind. However, expanding MH beyond cancer treatment requires novel AMF apparatus that can fully exploit the potential of magnetic nanoparticles and localized heating effects. Fig. 15 summarizes in a visual way the composition and AMF ranges used for biomedical and non-biomedical applications and compares them.

The integration of magnetic MH with imaging techniques like MRI, MPI, magneto-motive ultrasonography (MMUS) and magneto-photoacoustic imaging (MPAI) has shown significant potential for cancer therapy,[183,184] and yet applications beyond oncology are rarely explored. This combination enables precise, real-time tracking of therapeutic agents and localized heating, which will be essential for optimizing treatment efficacy and safety in diverse fields such as targeted drug delivery, tissue engineering, and regenerative medicine. By providing dynamic feedback on agent distribution and temperature control, the multimodal approach paves the way for more personalized and effective therapies across a wide range of medical conditions.

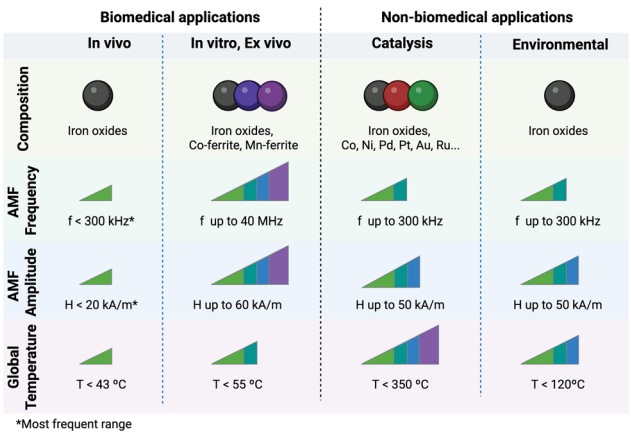

Fig. 15 Summary of the chemical compositions (iron oxides *vs.* other compositions), range of AMF conditions used (frequency and amplitude) and global temperatures reached for biomedical and non-biomedical applications. Figure created in Biorender.

Indeed, the combination of magnetic guidance and hyperthermia offers a promising approach for non-biomedical applications in which MNPs must act in wide open spaces, enabling targeted and efficient remediation processes. This is the case for environmental applications. The localized heat achieved through MH can be utilized to remove or neutralize pollutants.[185] For example, the motion ability of magnetic nanorobots significantly enhances the active capture of free-swimming Gram-negative bacteria, dispersed nano- and microplastics in aquatic environments,[186] persistent organic pollutants, heavy metals, oils, and pathogenic microorganisms. Dynamic capture is more efficient than static particles. In addition, the toxic contaminants adsorbed on the magnetic nanorobots can be disposed of by a simple cooling process and these exhibit good recovery retention after multiple reuse cycles.[187] This combination of temperature sensitive aggregation/separation coupled with magnetic propulsion (3 mT and frequency range of 0.5–4.0 Hz) opens a plethora of opportunities in the applicability of nanorobots for water treatment and targeted pollutant removal approaches. In this context, micro- and nanorobots guided by magnetic fields could have transformative potential not only for environmental applications, but also for most of the applications highlighted in this work.

However, a transversal trend that critically shapes the future of MH (across all applications) is scaling up both materials and devices. One persistent challenge is the reproducibility of nanoparticle synthesis,[188] as minor variations in parameters such as size, morphology, crystallinity, and surface chemistry can drastically affect heating performance. Fortunately, recent developments in controlled synthesis protocols, batch-to-batch consistency, and scalable production routes (*e.g.*, microwave-assisted and continuous-flow syntheses) have shown that high-quality MNPs with reliable magnetic and thermal profiles can be produced at larger scales.[144,189]

Similarly, the scale-up and engineering of magnetic hyperthermia setups present application-specific hurdles. In the biomedical domain, hardware must deliver sufficient power without exceeding safety thresholds to prevent tissue damage from eddy currents. Conversely, in industrial and environmental settings, where those biological constraints are relaxed, new challenges emerge, such as ensuring field homogeneity and heat uniformity across larger volumes, adapting coil geometries to fluid dynamics, and managing power consumption and cooling. To overcome these limitations, several strategies are gaining traction. Modular coil designs with

adjustable geometries (planar, solenoidal) and field profiles can enhance adaptability to different reactors.[190] The integration of embedded sensors and field mapping tools can improve thermal uniformity and system feedback. From a materials standpoint, controlled distribution of MNPs, *e.g.*, *via* fixed-bed reactors, enables localized heating where it is most needed while avoiding unnecessary thermal diffusion. In parallel, computational modeling of field distribution and heat transfer, combined with experimental validation, will be essential for informing large-scale system design. The adoption of open-access coil calibration protocols and shared platforms for hardware benchmarking could further facilitate reproducibility and cross-validation among research groups worldwide.

Finally, future trends in MH will depend not only on the creativity of material design or device engineering but on our ability to integrate these components into robust, scalable systems that respond to societal demands for non-toxic, efficient, and affordable technologies across both biomedical and non-biomedical frontiers.

Author contributions

The manuscript was written through contributions of all authors. All authors have given approval to the final version of the manuscript.

Conflicts of interest

There are no conflicts to declare.

Data availability

No primary research results, software or code have been included and no new data were generated or analysed as part of this review.

Acknowledgements

The authors would like to acknowledge funding from the "Plan de Recuperación, Transformación y Resiliencia" financed by the European Union–NextGenerationEU under H2umidity-Plus project; the Spanish Ministry of Science and Innovation through Project TED2021-130191B-C43, a Ramón y Cajal Research Fellowship (RYC2021-032448-I), and Project PID2023-150760NA-100; Project CNS2023-144321 funded by MICIU/AEI/10.13039/501100011033 and NextGenerationEU/PRTR; Fondo Social del Gobierno de Aragón (grupo DGA E15-23R); and the Severo Ochoa Centres of Excellence program through Grants CEX2023-001286-S and CEX2024-001445-S funded by MICIU/AEI/10.13039/501100011033. This publication is based upon work from COST Action CA23132 "MagneticParticle Imaging for next-generation theranostics and medical research" (NexMPI), supported by COST (European Cooperation in Science and Technology); and within the framework of the Una Europa Seed Funding Project DREAM-Nano (SF2405). A. P.-R. acknowledges funding from Beca Santander-Universidad de Zaragoza. Finally, the authors would like to thank the referees for their meticulous review, which contributed to improving this work.

References

1 A. Jordan, P. Wust, H. Fähling, W. John, A. Hinz and R. Felix, *Int. J. Hyperthermia*, 2009, **25**, 499–511.
2 A. Meffre, B. Mehdaoui, V. Connord, J. Carrey, P. F. Fazzini, S. Lachaize, M. Respaud and B. Chaudret, *Nano Lett.*, 2015, **15**, 3241–3248.
3 X. Yu, R. Yang, C. Wu, B. Liu and W. Zhang, *Sci. Rep.*, 2022, **12**, 16055.
4 S. Ruta, Y. Fernández-Alonso, S. E. Rannala, M. P. Morales, S. Veintemillas-Verdaguer, C. Jones, L. Gutiérrez, R. Chantrell and D. Serantes, *Nanoscale Adv.*, 2024, **6**, 4207–4218.
5 J. Wells, D. Ortega, U. Steinhoff, S. Dutz, E. Garaio, O. Sandre, E. Natividad, M. M. Cruz, F. Brero, P. Southern, Q. A. Pankhurst and S. Spassov, *Int. J. Hyperthermia*, 2021, **38**, 447–460.
6 R. R. Wildeboer, P. Southern and Q. A. Pankhurst, *J. Phys. D: Appl. Phys.*, 2014, **47**, 495003.
7 Y. Gu, R. Piñol, R. Moreno-Loshuertos, C. D. S. Brites, J. Zeler, A. Martínez, G. Maurin-Pasturel, P. Fernández-Silva, J. Marco-Brualla, P. Téllez, R. Cases, R. Navarro Belsué, D. Bonvin, L. D. Carlos and A. Millán, *ACS Nano*, 2023, **17**, 6822–6832.
8 A. Gupta, R. S. Kane and D.-A. Borca-Tasciuc, *J. Appl. Phys.*, 2010, **108**, 064901.
9 L. Polo-Corrales and C. Rinaldi, *J. Appl. Phys.*, 2012, **111**, 07B334.
10 S. Faure, N. Mille, S. S. Kale, J. M. Asensio, J. Marbaix, P. Farger, D. Stoian, W. Van Beek, P.-F. Fazzini, K. Soulantica, B. Chaudret and J. Carrey, *J. Phys. Chem. C*, 2020, **124**, 22259–22265.
11 D. Cabrera, A. Lak, T. Yoshida, M. E. Materia, D. Ortega, F. Ludwig, P. Guardia, A. Sathya, T. Pellegrino and F. J. Teran, *Nanoscale*, 2017, **9**, 5094–5101.
12 J. Dong and J. I. Zink, *ACS Nano*, 2014, **8**, 5199–5207.
13 L. M. Martínez-Prieto, J. Marbaix, J. M. Asensio, C. Cerezo-Navarrete, P.-F. Fazzini, K. Soulantica, B. Chaudret and A. Corma, *ACS Appl. Nano Mater.*, 2020, **3**, 7076–7087.
14 S. R. Yassine, Z. Fatfat, G. H. Darwish and P. Karam, *Catal. Sci. Technol.*, 2020, **10**, 3890–3896.
15 I. M. Marin, D. D. Masi, L. Lacroix, P. Fazzini, P. W. N. M. van Leeuwen, J. M. Asensio and B. Chaudret, *Green Chem.*, 2021, **23**, 2025–2036.
16 J. Mazarío, I. Mustieles Marin, G. Mencia, C. W. Lopes, V. Varela-Izquierdo, G. Agostini, P.-F. Fazzini, N. Ratel-Ramond and B. Chaudret, *ACS Appl. Mater. Interfaces*, 2024, **7**, 9412–9427.

17 S. Ceylan, C. Friese, C. Lammel, K. Mazac and A. Kirschning, *Angew. Chem., Int. Ed.*, 2008, **47**, 8950–8953.
18 B. Corrales-Pérez, G. Vicente, M. P. Morales and A. Gallo-Cordova, *Fuel*, 2024, **368**, 131659.
19 J. G. Ovejero, I. Armenia, D. Serantes, S. Veintemillas-Verdaguer, N. Zeballos, F. López-Gallego, C. Grüttner, J. M. de la Fuente, M. P. Morales and V. Grazu, *Nano Lett.*, 2021, **21**, 7213–7220.
20 M. Banchelli, S. Nappini, C. Montis, M. Bonini, P. Canton, D. Berti and P. Baglioni, *Phys. Chem. Chem. Phys.*, 2014, **16**, 10023.
21 C. Chen, L. Chen, Y. Yi, C. Chen, L.-F. Wu and T. Song, *Appl. Environ. Microbiol.*, 2016, **82**, 2219–2226.
22 R. T. Guntnur, N. Muzzio, A. Gomez, S. Macias, A. Galindo, A. Ponce and G. Romero, *Adv. Funct. Mater.*, 2022, **32**, 2204732.
23 J. Liu, X. Guo, Z. Zhao, B. Li, J. Qin, Z. Peng, G. He, D. J. L. Brett, R. Wang and X. Lu, *Appl. Mater. Today*, 2020, **18**, 100457.
24 J. Marbaix, N. Mille, J. Carrey, K. Soulantica and B. Chaudret, in *Nanoparticles in Catalysis*, John Wiley & Sons, Ltd, 2021, pp. 307–329.
25 I. F. Pinheiro, M. E. F. Brollo, G. S. Bassani, G. Varet, D. Merino-Garcia, V. C. B. Guersoni, M. Knobel, A. C. Bannwart, D. Muraca and C. van der Geest, *Fuel*, 2023, **331**, 125810.
26 J. A. Fuentes-García, B. Sanz, R. Mallada, M. R. Ibarra and G. F. Goya, *Mater. Des.*, 2023, **226**, 111615.
27 M. U. Farid, J. A. Kharraz, S. Sharma, R. J. Khan, N. K. Khanzada, B. J. Deka, M. K. Nallapaneni, S. S. Chopra, S.-Y. Leu, S. W. Hasan, N. Hilal and A. K. J. An, *Desalination*, 2024, **574**, 117235.
28 S. Dutz and R. Hergt, *Int. J. Hyperthermia*, 2013, **29**, 790–800.
29 A. García-Zaragoza, J. L. Del Río-Rodríguez, C. Cerezo-Navarrete, S. Gutiérrez-Tarriño, M. A. Molina, L. Costley-Wood, J. Mazarío, B. Chaudret, L. M. Martínez-Prieto, A. M. Beale and P. Oña-Burgos, *ACS Catal.*, 2025, **15**, 9489–9502.
30 S. Lin, W. Hetaba, B. Chaudret, W. Leitner and A. Bordet, *Adv. Energy Mater.*, 2022, **12**, 2270173.
31 J. Kim, J. Wang, H. Kim and S. Bae, *Sci. Rep.*, 2021, **11**, 733.
32 R. E. Rosensweig, *J. Magn. Magn. Mater.*, 2002, **252**, 370–374.
33 C. Wang, N. Chen, T. Yang, Q. Cheng, D. Wu, Y. Xiao, S. He and N. Song, *J. Magn. Magn. Mater.*, 2023, **565**, 170267.
34 J. Sommertune, A. Sugunan, A. Ahniyaz, R. Bejhed, A. Sarwe, C. Johansson, C. Balceris, F. Ludwig, O. Posth and A. Fornara, *Int. J. Mol. Sci.*, 2015, **16**, 19752–19768.
35 Y. Sapir-Lekhovitser, M. Y. Rotenberg, J. Jopp, G. Friedman, B. Polyak and S. Cohen, *Nanoscale*, 2016, **8**, 3386–3399.
36 H. Gavilán, S. K. Avugadda, T. Fernández-Cabada, N. Soni, M. Cassani, B. T. Mai, R. Chantrell and T. Pellegrino, *Chem. Soc. Rev.*, 2021, **50**, 11614–11667.
37 C. Martinez-Boubeta, K. Simeonidis, A. Makridis, M. Angelakeris, O. Iglesias, P. Guardia, A. Cabot, L. Yedra, S. Estradé, F. Peiró, Z. Saghi, P. A. Midgley, I. Conde-Leborán, D. Serantes and D. Baldomir, *Sci. Rep.*, 2013, **3**, 1652.
38 D. Egea-Benavente, C. Díaz-Ufano, Á. Gallo-Cordova, F. J. Palomares, J. L. Cuya Huaman, D. F. Barber, M. P. Morales and J. Balachandran, *ACS Appl. Mater. Interfaces*, 2023, **15**, 32162–32176.
39 J. Borchers, K. Krycka, B. Bosch-Santos, E. De Lima Correa, A. Sharma, H. Carlton, Y. Dang, M. Donahue, C. Grüttner, R. Ivkov and C. L. Dennis, *Small Struct.*, 2025, **6**, 2400410.
40 H. Gavilán, K. Simeonidis, E. Myrovali, E. Mazarío, O. Chubykalo-Fesenko, R. Chantrell, L. l. Balcells, M. Angelakeris, M. P. Morales and D. Serantes, *Nanoscale*, 2021, **13**, 15631–15646.
41 J. G. Ovejero, F. Spizzo, M. P. Morales and L. Del Bianco, *Materials*, 2021, **14**, 6416.
42 A. Lak, M. Cassani, B. T. Mai, N. Winckelmans, D. Cabrera, E. Sadrollahi, S. Marras, H. Remmer, S. Fiorito, L. Cremades-Jimeno, F. J. Litterst, F. Ludwig, L. Manna, F. J. Teran, S. Bals and T. Pellegrino, *Nano Lett.*, 2018, **18**, 6856–6866.
43 E. Fantechi, C. Innocenti, M. Albino, E. Lottini and C. Sangregorio, *J. Magn. Magn. Mater.*, 2015, **380**, 365–371.
44 A. Zeleňáková, Ľ. Nagy, P. Hrubovčák, M. Barutiak, M. Lisnichuk, V. Huntošová, A. Mrakovič, M. Gerina and D. Zákutná, *J. Alloys Compd.*, 2024, **989**, 174415.
45 R. Sahayaraj, K. Enoch, S. S. Pati and A. A. Somasundaram, *Ceram. Int.*, 2025, **51**, 20786–20797.
46 J. Marbaix, N. Mille, L.-M. Lacroix, J. M. Asensio, P.-F. Fazzini, K. Soulantica, J. Carrey and B. Chaudret, *ACS Appl. Nano Mater.*, 2020, **3**, 3767–3778.
47 K. Dev, A. Kadian, V. Manikandan, M. Pant, A. K. Mahapatro and S. Annapoorni, *Mater. Today Commun.*, 2025, **43**, 111669.
48 R. E. Camley, Z. Celinski and R. L. Stamps, *Magnetism of Surfaces, Interfaces, and Nanoscale Materials*, Elsevier, 1st edn, 2015, vol. 5.
49 G. Niraula, C. Wu, X. Yu, S. Malik, D. S. Verma, R. Yang, B. Zhao, S. Ding, W. Zhang and S. K. Sharma, *J. Mater. Chem. B*, 2024, **12**, 286–331.
50 R. Ferrero, M. Vicentini and A. Manzin, *Nanoscale Adv.*, 2024, **6**, 1739–1749.
51 M. Smari, M. V. Moisiuc, M. Y. Al-Haik, I. Astefanoaei, A. Stancu, F. Shelkovyi, R. Gimaev, J. Piashova, V. Zverev and Y. Haik, *Nanomaterials*, 2025, **15**, 642.
52 I. Obaidat, B. Issa and Y. Haik, *Nanomaterials*, 2015, **5**, 63–89.
53 P. F. De Châtel, I. Nándori, J. Hakl, S. Mészáros and K. Vad, *J. Phys.: Condens. Matter*, 2009, **21**, 124202.
54 J. Mazarío, S. Ghosh, V. Varela-Izquierdo, L. M. Martínez-Prieto and B. Chaudret, *ChemCatChem*, 2025, **17**, e202400683.
55 J. Wells, O. Kosch and F. Wiekhorst, *J. Magn. Magn. Mater.*, 2022, **563**, 169992.

56 D. Kouzoudis, G. Samourgkanidis, A. Kolokithas-Ntoukas, G. Zoppellaro and K. Spiliotopoulos, *Front. Mater.*, 2021, **8**, 638019.
57 A. Mohapatra, M. A. Harris, D. LeVine, M. Ghimire, J. A. Jennings, B. I. Morshed, W. O. Haggard, J. D. Bumgardner, S. R. Mishra and T. Fujiwara, *J. Biomed. Mater. Res.*, 2018, **106**, 2169–2176.
58 M. Harris, H. Ahmed, B. Barr, D. Levine, L. Pace, A. Mohapatra, B. Morshed, J. D. Bumgardner and J. A. Jennings, *Int. J. Biol. Macromol.*, 2017, **104**, 1407–1414.
59 T. Wu, L. Wang, M. Gong, Y. Lin, Y. Xu, L. Ye, X. Yu, J. Liu, J. Liu, S. He, H. Zeng and G. Wang, *J. Magn. Magn. Mater.*, 2019, **485**, 95–104.
60 A. Bigham, A. H. Aghajanian, S. Behzadzadeh, Z. Sokhani, S. Shojaei, Y. Kaviani and S. A. Hassanzadeh-Tabrizi, *Mater. Sci. Eng., C*, 2019, **99**, 83–95.
61 B. M. Salah, M. Rady, M. Abdel-Halim, H. M. Fahmy, N. S. El-Din and M. H. Gaber, *Biophysics*, 2021, **66**, 264–272.
62 L. García, E. Garaio, A. López-Ortega, I. Galarreta-Rodriguez, L. Cervera-Gabalda, G. Cruz-Quesada, A. Cornejo, J. J. Garrido, C. Gómez-Polo and J. I. Pérez-Landazábal, *Langmuir*, 2023, **39**, 211–219.
63 W. M. O. S. De Santana, S. Abramson, R. Fini, B. L. Caetano, C. Ménager, S. H. Pulcinelli and C. V. Santilli, *ACS Appl. Polym. Mater.*, 2021, **3**, 4837–4848.
64 S. R. Ansari, N.-J. Hempel, S. Asad, P. Svedlindh, C. A. S. Bergström, K. Löbmann and A. Teleki, *ACS Appl. Mater. Interfaces*, 2022, **14**, 21978–21988.
65 L. Mandić, M. Matković, G. Baranović and S. Šegota, *Antioxidants*, 2023, **12**, 732.
66 J. Wang, Q. Zhou, Q. Dong, J. Shen, J. Hao, D. Li, T. Xu, X. Cai, W. Bai, T. Ying, Y. Li, L. Zhang, Y. Zhu, L. Wang, J. Wu and Y. Zheng, *Small*, 2024, **20**, 2400408.
67 A. B. Santi, N. Muzzio, A. Gomez and G. Romero, *ACS Appl. Nano Mater.*, 2025, **8**, 7899–7910.
68 J. Wang, G. Zhao, Z. Zhang, X. Xu and X. He, *Acta Biomater.*, 2016, **33**, 264–274.
69 T. Wakabayashi, M. Kaneko, T. Nakai, M. Horie, H. Fujimoto, M. Takahashi, S. Tanoue and A. Ito, *Bioeng. Transl. Med.*, 2023, **8**, e10416.
70 Z. Han, J. S. Rao, L. Gangwar, B.-E. Namsrai, J. L. Pasek-Allen, M. L. Etheridge, S. M. Wolf, T. L. Pruett, J. C. Bischof and E. B. Finger, *Nat. Commun.*, 2023, **14**, 3407.
71 A. Chiu-Lam, E. Staples, C. J. Pepine and C. Rinaldi, *Sci. Adv.*, 2021, **7**, eabe3005.
72 P. Chen, S. Wang, Z. Chen, P. Ren, R. G. Hepfer, E. D. Greene, L. H. Campbell, K. L. Helke, X. Nie, J. H. Jensen, C. Hill, Y. Wu, K. G. M. Brockbank and H. Yao, *Commun. Biol.*, 2023, **6**, 1–13.
73 Z. Luo, T. Shi, Z. Ruan, C. Ding, R. Huang, W. Wang, Z. Guo, Z. Zhan, Y. Zhang and Y. Chen, *Small*, 2024, **20**, 2304836.
74 S. Singh, K. C. Barick and D. Bahadur, *Powder Technol.*, 2015, **269**, 513–519.
75 C. J. L. Murray, K. S. Ikuta, F. Sharara, L. Swetschinski, *et al.*, *The Lancet.*, 2022, **399**, 629–655.
76 Y. Jabalera, M. Montalban-Lopez, J. J. Vinuesa-Rodriguez, G. R. Iglesias, M. Maqueda and C. Jimenez-Lopez, *Int. J. Biol. Macromol.*, 2021, **189**, 206–213.
77 M. Bañobre-López, D. Rodrigues, B. Espiña, J. Azeredo and J. Rivas, *IEEE Trans. Magn.*, 2013, **49**, 3508–3511.
78 H. Huang, S. Delikanli, H. Zeng, D. M. Ferkey and A. Pralle, *Nat. Nanotechnol.*, 2010, **5**, 602–606.
79 J. Idiago-López, D. Ferreira, L. Asín, M. Moros, I. Armenia, V. Grazú, A. R. Fernandes, J. M. de la Fuente, P. V. Baptista and R. M. Fratila, *Nanoscale*, 2024, **16**, 15176–15195.
80 R. Chen, G. Romero, M. G. Christiansen, A. Mohr and P. Anikeeva, *Science*, 2015, **347**, 1477–1480.
81 R. Munshi, S. M. Qadri, Q. Zhang, I. Castellanos Rubio, P. del Pino and A. Pralle, *eLife*, 2017, **6**, e27069.
82 M.-C. Horny, V. Dupuis, J.-M. Siaugue and J. Gamby, *Sensors*, 2021, **21**, 185.
83 S. Lopez, N. Hallali, Y. Lalatonne, A. Hillion, J. C. Antunes, N. Serhan, P. Clerc, D. Fourmy, L. Motte, J. Carrey and V. Gigoux, *Nanoscale Adv.*, 2022, **4**, 421–436.
84 P. Kulshrestha, M. Gogoi, D. Bahadur and R. Banerjee, *Colloids Surf., B*, 2012, **96**, 1–7.
85 M. E. Fortes Brollo, A. Domínguez-Bajo, A. Tabero, V. Domínguez-Arca, V. Gisbert, G. Prieto, C. Johansson, R. Garcia, A. Villanueva, M. C. Serrano and M. D. P. Morales, *ACS Appl. Mater. Interfaces*, 2020, **12**, 4295–4307.
86 N. S. Satarkar and J. Z. Hilt, *J. Controlled Release*, 2008, **130**, 246–251.
87 K. Fukukawa, Y. Shibasaki and M. Ueda, *Polym. Adv. Technol.*, 2006, **17**, 131–136.
88 F. Crippa, T. L. Moore, M. Mortato, C. Geers, L. Haeni, A. M. Hirt, B. Rothen-Rutishauser and A. Petri-Fink, *J. Magn. Magn. Mater.*, 2017, **427**, 212–219.
89 S. Nappini, F. B. Bombelli, M. Bonini, B. Nordèn and P. Baglioni, *Soft Matter*, 2009, **6**, 154–162.
90 Y. Chen, A. Bose and G. D. Bothun, *ACS Nano*, 2010, **4**, 3215–3221.
91 G. Podaru, S. Ogden, A. Baxter, T. Shrestha, S. Ren, P. Thapa, R. K. Dani, H. Wang, M. T. Basel, P. Prakash, S. H. Bossmann and V. Chikan, *J. Phys. Chem. B*, 2014, **118**, 11715–11722.
92 R. Wardlow, C. Bing, J. VanOsdol, D. Maples, M. Ladouceur-Wodzak, M. Harbeson, J. Nofiele, R. Staruch, A. Ramachandran, J. Malayer, R. Chopra and A. Ranjan, *Int. J. Hyperthermia*, 2016, **32**, 254–264.
93 B. Fan, J. F. Trant, G. Hemery, O. Sandre and E. R. Gillies, *Chem. Commun.*, 2017, **53**, 12068–12071.
94 GBD 2016 Causes of Death Collaborators, *Lancet*, 2017, **390**, 1151–1210.
95 G. Chinetti-Gbaguidi, S. Colin and B. Staels, *Nat. Rev. Cardiol.*, 2015, **12**, 10–17.
96 M. E. Kooi, V. C. Cappendijk, K. B. J. M. Cleutjens, A. G. H. Kessels, P. J. Kitslaar, M. Borgers, P. M. Frederik, M. J. A. P. Daemen and J. M. A. Van Engelshoven, *Circulation*, 2003, **107**, 2453–2458.

97 L. Li, R. Wang, H.-H. Shi, L. Xie, J.-D.–S. Li, W.-C. Kong, J.-T. Tang, D.-N. Ke and L.-Y. Zhao, *Exp. Ther. Med.*, 2013, **6**, 347–354.
98 C. K. Black, K. M. Termanini, O. Aguirre, J. S. Hawksworth and M. Sosin, *Ann. Transl. Med.*, 2018, **6**, 409.
99 N. Manuchehrabadi, Z. Gao, J. Zhang, H. L. Ring, Q. Shao, F. Liu, M. McDermott, A. Fok, Y. Rabin, K. G. M. Brockbank, M. Garwood, C. L. Haynes and J. C. Bischof, *Sci. Transl. Med.*, 2017, **9**(379), eaah4586.
100 F. M. Guttman, J. Lizin, P. Robitaille, H. Blanchard and C. Turgeon-Knaack, *Cryobiology*, 1977, **14**, 559–567.
101 P. Joshi, L. E. Ehrlich, Z. Gao, J. C. Bischof and Y. Rabin, *J. Heat Transfer*, 2022, **144**, 031202.
102 S. Karimi, S. N. Tabatabaei, M. G. Novin, M. Kazemi, Z. S. Mofarahe and A. Ebrahimzadeh-Bideskan, *Heliyon*, 2023, **9**, e18828.
103 C. J. L. Murray, K. S. Ikuta, F. Sharara, L. Swetschinski, *et al.*, *The Lancet*, 2022, **399**(10325), 629–655.
104 G. Tommasini, S. D. Sol-Fernández, A. C. Flavián-Lázaro, A. Lewinska, M. Wnuk, C. Tortiglione and M. Moros, *Adv. Funct. Mater.*, 2024, **34**, 2405282.
105 *The Bacterial Flagellum: Methods and Protocols*, ed. T. Minamino and K. Namba, Springer New York, New York, NY, 2017, vol. 1593.
106 S. Sol-Fernández, P. Martínez-Vicente, P. Gomollón-Zueco, C. Castro-Hinojosa, L. Gutiérrez, R. M. Fratila and M. Moros, *Nanoscale*, 2022, **14**, 2091–2118.
107 D. E. Clapham, *Nature*, 2003, **426**, 517–524.
108 A. D. Güler, H. Lee, T. Iida, I. Shimizu, M. Tominaga and M. Caterina, *J. Neurosci.*, 2002, **22**, 6408–6414.
109 S. A. Stanley, J. E. Gagner, S. Damanpour, M. Yoshida, J. S. Dordick and J. M. Friedman, *Science*, 2012, **336**, 604–608.
110 J. P. M. White, M. Cibelli, L. Urban, B. Nilius, J. G. McGeown and I. Nagy, *Physiol. Rev.*, 2016, **96**, 911–973.
111 S. A. Stanley, J. Sauer, R. S. Kane, J. S. Dordick and J. M. Friedman, *Nat. Med.*, 2015, **21**, 92–98.
112 S. A. Stanley, L. Kelly, K. N. Latcha, S. F. Schmidt, X. Yu, A. R. Nectow, J. Sauer, J. P. Dyke, J. S. Dordick and J. M. Friedman, *Nature*, 2016, **531**, 647–650.
113 M. Meister, *eLife*, 2016, **5**, e17210.
114 K. K. Zhu, I. Gispert Contamina, O. Ces, L. M. C. Barter, J. W. Hindley and Y. Elani, *J. Am. Chem. Soc.*, 2024, **146**, 13176–13182.
115 M. Kim, J. D. Nicholas, J. Puigmartí-Luis, B. J. Nelson and S. Pané, *Annu. Rev. Control Robot. Auton. Syst.*, 2025, **8**, 379–405.
116 A. Elnaggar, S. Kang, M. Tian, B. Han and M. Keshavarz, *Small Sci.*, 2024, **4**, 2300211.
117 L. Zhang, M. Pumera, S. Sánchez and X. Ma, *Nanoscale*, 2024, 19936.
118 R. Gao, W. Zhang, X. Chen, J. Shen, Y. Qin, Y. Wang, X. Wei, W. Zou, X. Jiang, Y. Wang, W. Huang, H. Chen, Z. Li, H. Fan, B. He and Y. Cheng, *ACS Nano*, 2024, **18**, 29492–29506.
119 J. Chen and Y. Wang, *Nanotechnology*, 2020, **31**, 495706.
120 S. N. Tabatabaei, H. Girouard, A.-S. Carret and S. Martel, *J. Controlled Release*, 2015, **206**, 49–57.
121 A. Bordet, W. Leitner and B. Chaudret, *Angew. Chem., Int. Ed.*, 2025, **64**, e202424151.
122 W. Wang, G. Tuci, C. Duong-Viet, Y. Liu, A. Rossin, L. Luconi, J.-M. Nhut, L. Nguyen-Dinh, C. Pham-Huu and G. Giambastiani, *ACS Catal.*, 2019, **9**, 7921–7935.
123 D. Astruc, F. Lu and J. R. Aranzaes, *Angew. Chem., Int. Ed.*, 2005, **44**, 7852–7872.
124 K. Philippot and A. Roucoux, *Nanoparticles in Catalysis: Advances in Synthesis and Applications*, John Wiley & Sons., 2021.
125 S. R. Chaudhuri, J. Hartwig, L. Kupracz, T. Kodanek, J. Wegner and A. Kirschning, *Adv. Synth. Catal.*, 2014, **356**, 3530–3538.
126 P. M. Mortensen, J. S. Engbæk, S. B. Vendelbo, M. F. Hansen and M. Østberg, *Ind. Eng. Chem. Res.*, 2017, **56**, 14006–14013.
127 D. D. Masi, J. M. Asensio, P. F. Fazzini, L. M. Lacroix and B. Chaudret, *Angew. Chem., Int. Ed.*, 2020, **59**, 6187–6191.
128 S. S. Kale, J. M. Asensio, M. Estrader, M. Werner, A. Bordet, D. Yi, J. Marbaix, P.-F. Fazzini, K. Soulantica and B. Chaudret, *Catal. Sci. Technol.*, 2019, **9**, 2601–2607.
129 T. Tatarchuk, A. Shyichuk, N. Danyliuk, M. Naushad, V. Kotsyubynsky and V. Boychuk, *Chemosphere*, 2023, **326**, 138364.
130 F. L. Rivera, F. J. Recio, F. J. Palomares, J. Sánchez-Marcos, N. Menéndez, E. Mazarío and P. Herrasti, *J. Electroanal. Chem.*, 2020, **879**, 114773.
131 A. Gallo-Cordova, J. J. Castro, E. L. Winkler, E. Lima, R. D. Zysler, M. P. Morales, J. G. Ovejero and D. A. Streitwieser, *J. Cleaner Prod.*, 2021, **308**, 127385.
132 A. Gallo-Cordova, S. Veintemillas-Verdaguer, P. Tartaj, E. Mazarío, M. P. Morales and J. G. Ovejero, *Nanomaterials*, 2021, **11**, 1052.
133 C. Niether, S. Faure, A. Bordet, J. Deseure, M. Chatenet, J. Carrey, B. Chaudret and A. Rouet, *Nat. Energy*, 2018, **3**, 476–483.
134 J. M. Asensio, A. B. Miguel, P.-F. Fazzini, P. W. N. M. van Leeuwen and B. Chaudret, *Angew. Chem.*, 2019, **131**, 11428–11432.
135 C. Cerezo-Navarrete, I. M. Marin, H. García-Miquel, A. Corma, B. Chaudret and L. M. Martínez-Prieto, *ACS Catal.*, 2022, **12**, 8462–8475.
136 M. G. Vinum, M. R. Almind, J. S. Engbæk, S. B. Vendelbo, M. F. Hansen, C. Frandsen, J. Bendix and P. M. Mortensen, *Angew. Chem., Int. Ed.*, 2018, **57**, 10569–10573.
137 Z. Ma, J. Mohapatra, K. Wei, J. P. Liu and S. Sun, *Chem. Rev.*, 2023, **123**, 3904–3943.
138 R. Piner, H. Li, X. Kong, L. Tao, I. N. Kholmanov, H. Ji, W. H. Lee, J. W. Suk, J. Ye, Y. Hao, S. Chen, C. W. Magnuson, A. F. Ismach, D. Akinwande and R. S. Ruoff, *ACS Nano*, 2013, **7**, 7495–7499.
139 E. Roduner, *Chem. Soc. Rev.*, 2014, **43**, 8226–8239.

140 N. S. Moura, K. R. Bajgiran, C. L. Roman, L. Daemen, Y. Cheng, J. Lawrence, A. T. Melvin, K. M. Dooley and J. A. Dorman, *ChemSusChem*, 2021, **14**, 1122–1130.
141 C. Biz, J. Gracia and M. Fianchini, *Int. J. Mol. Sci.*, 2022, **23**, 1–68.
142 A. Fache, F. Marias and B. Chaudret, *Chem. Eng. J.*, 2020, **390**, 124531.
143 G. N. Lucena, C. C. dos Santos, G. C. Pinto, R. D. Piazza, W. N. Guedes, M. Jafelicci Júnior, A. V. de Paula and R. F. C. Marques, *J. Magn. Magn. Mater.*, 2020, **516**, 167326.
144 A. Gallo-Cordova, B. Corrales-Pérez, P. Cabrero, C. Force, S. Veintemillas-Verdaguer, J. G. Ovejero and M. P. Morales, *Chem. Eng. J.*, 2024, **490**, 151725.
145 G. R. Eaton, S. S. Eaton, D. P. Barr and R. T. Weber, *Quantitative EPR*, Springer, Vienna, 2010.
146 B. Bouvet, S. Sene, G. Félix, J. Havot, G. Audran, S. R. A. Marque, J. Larionova and Y. Guari, *Nanoscale*, 2022, **15**, 144–153.
147 Y.-X. Ge, P.-Y. Zhu, Y. Yu, L.-C. Zhang, C. Zhang and L. Liu, *J. Mater. Chem. A*, 2022, **10**, 23314–23322.
148 J. L. Del Rio-Rodríguez, S. Gutiérrez-Tarriño, I. Márquez, Á. Gallo-Cordova, M. A. Molina, J. S. Martínez, J. J. Calvente, C. Cerezo-Navarrete, A. M. Beale, M. P. Morales, J. L. Olloqui-Sariego and P. Oña-Burgos, *Small*, 2025, **21**, 2503871.
149 T. Li, S. Kang, S. Li, W. Yang, W. Lei, W. Lu, Z. Li, D. Zhu, X. Zhang and P. Lei, *J. Phys. D: Appl. Phys.*, 2025, **58**, 125504.
150 O. A. Mawlid, H. H. Abdelhady and M. S. El-Deab, *Energy Fuels*, 2024, **38**, 20169–20195.
151 S. Tamjidi, H. Esmaeili and B. K. Moghadas, *J. Cleaner Prod.*, 2021, **305**, 127200.
152 P. T. Sekoai, C. N. M. Ouma, S. P. Du Preez, P. Modisha, N. Engelbrecht, D. G. Bessarabov and A. Ghimire, *Fuel*, 2019, **237**, 380–397.
153 S. G. Krishnan, F. Pua and F. Zhang, *Biomass Bioenergy*, 2021, **149**, 106099.
154 J. Mazarío, V. Varela-Izquierdo and B. Chaudret, in *Surface Functionalized Metal Catalysts*, ed. L. M. Martínez-Prieto, Springer Nature Switzerland, Cham, 2024, pp. 243–271.
155 T. Phenrat, T. Thongboot and G. V. Lowry, *Environ. Sci. Technol.*, 2016, **50**, 872–880.
156 K. Yu, X. Yang, M. Wan, H. Jiang, P. Shao, L. Yang, H. Shi and X. Luo, *J. Hazard. Mater.*, 2023, **442**, 130019.
157 I. Kim, C. Best and S. Kim, *Geotech. Lett.*, 2020, **10**, 149–154.
158 H. Nguyen, N. Ohannesian, P. C. Bandara, A. Ansari, C. T. Deleo, D. Rodrigues, K. S. Martirosyan and W.-C. Shih, *ACS Appl. Mater. Interfaces*, 2020, **12**, 10291–10298.
159 A. Anvari, K. M. Kekre, A. Azimi Yancheshme, Y. Yao and A. Ronen, *J. Membr. Sci.*, 2019, **589**, 117253.
160 X. Lin, B. Shao, J. Zhu, F. Pan, J. Hu, M. Wang and H. Liu, *Energy Fuels*, 2020, **34**, 14439–14446.
161 M. Bellusci, A. Masi, M. Albino, D. Peddis, M. Petrecca, C. Sangregorio, A. La Barbera and F. Varsano, *Microporous Mesoporous Mater.*, 2021, **328**, 111458.
162 H. Li, M. M. Sadiq, K. Suzuki, R. Ricco, C. Doblin, A. J. Hill, S. Lim, P. Falcaro and M. R. Hill, *Adv. Mater.*, 2016, **28**, 1839–1844.
163 H. Li, M. M. Sadiq, K. Suzuki, C. Doblin, S. Lim, P. Falcaro, A. J. Hill and M. R. Hill, *J. Mater. Chem. A*, 2016, **4**, 18757–18762.
164 M. M. Sadiq, H. Li, A. J. Hill, P. Falcaro, M. R. Hill and K. Suzuki, *Chem. Mater.*, 2016, **28**, 6219–6226.
165 S. Wang and M. W. Urban, *Nat. Rev. Mater.*, 2020, **5**, 562–583.
166 T. Duenas, A. Enke, K. Chai, M. Castellucci, V. B. Sundaresan, F. Wudl, E. B. Murphy, A. Mal, J. R. Alexandar, A. Corder and T. K. Ooi, in *ACS Symposium Series*, ed. J. Baghdachi and T. Provder, American Chemical Society, Washington, DC, 2010, vol. 1050, pp. 45–60.
167 B. J. Adzima, C. J. Kloxin and C. N. Bowman, *Adv. Mater.*, 2010, **22**, 2784–2787.
168 C. C. Corten and M. W. Urban, *Adv. Mater.*, 2009, **21**, 5011–5015.
169 A. S. Ahmed and R. V. Ramanujan, *J. Mater. Res.*, 2015, **30**, 946–958.
170 Y. Yang, J. He, Q. Li, L. Gao, J. Hu, R. Zeng, J. Qin, S. X. Wang and Q. Wang, *Nat. Nanotechnol.*, 2019, **14**, 151–155.
171 R. Xu, G. S. Cañón Bermúdez, O. V. Pylypovskyi, O. M. Volkov, E. S. Oliveros Mata, Y. Zabila, R. Illing, P. Makushko, P. Milkin, L. Ionov, J. Fassbender and D. Makarov, *Nat. Commun.*, 2022, **13**, 6587.
172 H. Tao, D. Yue and C. Li, *Macromol. Mater. Eng.*, 2022, **307**, 2100649.
173 M. A. González Fernández, R. Bezerra De Melo, L. M. Fraga Trillo, S. Veintemillas Verdaguer, A. Gallo Córdova and M. P. Morales Herrero, *WO Pat.*, 2021116008A1, 2021.
174 N. García Saggion, Y. Rojas Pérez, R. Martín Negri and N. B. D'Accorso, in *Fundamentals and Industrial Applications of Magnetic Nanoparticles*, ed. C. M. Hussain and K. K. Patankar, Woodhead Publishing, 2022, pp. 555–597.
175 M. E. F. Brollo, I. F. Pinheiro, G. S. Bassani, G. Varet, V. C. B. Guersoni, M. Knobel, A. C. Bannwart, D. Muraca and C. van der Geest, *ACS Appl. Nano Mater.*, 2021, **4**, 13633–13642.
176 M. E. F. Brollo, I. F. Pinheiro, G. S. Bassani, G. Varet, D. Merino-Garcia, V. C. B. Guersoni, M. Knobel, A. C. Bannwart, C. van der Geest and D. Muraca, *ACS Omega*, 2023, **8**, 32520–32525.
177 K. C. B. Maia, A. D. D. S. Francisco, M. P. Moreira, R. S. V. Nascimento and D. Grasseschi, *ACS Omega*, 2024, **9**, 36874–36903.
178 Y. Song, L.-A. Shi, H. Xing, K. Jiang, J. Ge, L. Dong, Y. Lu and S.-H. Yu, *Adv. Mater.*, 2021, **33**, 2100074.
179 P. Clerc, P. Jeanjean, N. Hallali, M. Gougeon, B. Pipy, J. Carrey, D. Fourmy and V. Gigoux, *J. Controlled Release*, 2018, **270**, 120–134.
180 A. L. Miranda-Vilela, R. C. A. Peixoto, J. P. F. Longo, D. D. O. S. Cintra, F. A. Portilho, K. L. C. Miranda,

P. P. C. Sartoratto, S. N. Báo, R. B. De Azevedo and Z. G. M. Lacava, *J. Biomed. Nanotechnol.*, 2013, **9**, 1261–1271.
181 G. Niraula, C. Wu, X. Yu, S. Malik, D. S. Verma, R. Yang, B. Zhao, S. Ding, W. Zhang and S. K. Sharma, *J. Mater. Chem. B*, 2024, **12**, 286–331.
182 M. K. Y. Kwok, C. C. J. Maley, A. Dworkin, S. Hattersley, P. Southern and Q. A. Pankhurst, *App. Phys. Lett.*, 2023, **122**, 240502.
183 A. Shakeri-Zadeh and J. W. M. Bulte, *Nat. Rev. Bioeng.*, 2024, **3**, 245–260.
184 Y. Du, X. Liu, Q. Liang, X.-J. Liang and J. Tian, *Nano Lett.*, 2019, **19**, 3618–3626.
185 H. Zhou, C. C. Mayorga-Martinez, S. Pané, L. Zhang and M. Pumera, *Chem. Rev.*, 2021, **121**, 4999–5041.
186 M. Ussia, M. Urso, C. M. Oral and M. Pumera, *ACS Nano*, 2024, **18**, 13171–13183.
187 J. V. Vaghasiya, C. C. Mayorga-Martinez, S. Matějková and M. Pumera, *Nat. Commun.*, 2022, **13**, 1026.
188 I. Rubia-Rodríguez, A. Santana-Otero, S. Spassov, *et al.*, *Materials*, 2021, **14**, 706.
189 H. Gavilán, G. M. R. Rizzo, N. Silvestri, B. T. Mai and T. Pellegrino, *Nat. Protoc.*, 2023, **18**, 783–809.
190 M. Vicentini, R. Ferrero and A. Manzin, *Int. J. Therm. Sci.*, 2024, **203**, 109151.